ORNL--6242

DE86 004661

MODELING OF COMPLEX MELTING AND SOLIDIFICATION BEHAVIOR IN LASER-IRRADIATED MATERIALS

[A Description and User's Guide to the LASER8 Computer Program]

G. A. Geist and R. F. Wood

Date Published: November 1985

Research supported by the Exploratory Studies Program
of Oak Ridge National Laboratory
and by the Division of Materials Sciences
U.S. Department of Energy

Prepared by the
OAK RIDGE NATIONAL LABORATORY
Oak Ridge, Tennessee 37831
operated by
MARTIN MARIETTA ENERGY SYSTEMS, INC.
for the
U.S. DEPARTMENT OF ENERGY
under Contract No. DE-AC05-84OR21400

TABLE OF CONTENTS

MODELING OF COMPLEX MELTING AND SOLIDIFICATION BEHAVIOR IN LASER-IRRADIATED MATERIALS

[A Description and Users Guide to the LASER8 Computer Program]

G. A. Geist
Engineering Physics and Mathematics Division, Oak Ridge National Laboratory
Oak Ridge, Tennessee 37831

and

R. F. Wood
Solid State Division, Oak Ridge National Laboratory
Oak Ridge, Tennessee 37831

ABSTRACT

The conceptual foundation of a computational model and a computer program based on it have been developed for treating various aspects of the complex melting and solidification behavior observed in pulsed laser-irradiated materials. A particularly important feature of the modeling is the capability of allowing melting and solidification to occur at temperatures other than the thermodynamic phase change temperatures. As a result, interfacial undercooling and overheating can be introduced and various types of nucleation events can be simulated. Calculations on silicon with the model have shown a wide variety of behavior, including the formation and propagation of multiple phase fronts. Although originally developed as a tool for studying certain problems arising in the field of laser annealing of semiconductors, the program should be useful in treating many types of systems in which phase changes and nucleation phenomena play important roles.

This report describes the underlying physical and mathematical ideas and the basic relations used in LASER8. It also provides enough specific and detailed information on the program to serve as a guide for its use; a listing of one version of the program is given as an appendix.

1.0 Introduction

In the work described here we developed a mathematical model and a computer program, called LASER8, for the study of heat conduction and phase change problems arising in connection with the pulsed-laser irradiation of semiconductors.[1] The need for a program like LASER8 arose because of the inability of existing programs, such as HEATING5,[2-4] to treat phase-change problems with sufficient generality. This difficulty is overcome in LASER8 through the innovation of the state array concept, through which the state of the material in each small volume element is continuously monitored and controlled. We expect LASER8 to be particularly useful in the study of a wide class of problems in which melting and solidification of any material occur so rapidly that overheating and/or undercooling of the parent phase cannot be neglected. LASER8 also contains provisions for simulating bulk and surface nucleation effects under certain conditions. As far as we know, these are unique capabilities in a computer code and should be of widespread interest for a variety of problems. However, it should be recognized that nucleation theory is still primarily phenomenological and requires much further development to be put on a firm theoretical basis.

LASER8 is presently restricted to treating problems that can be approximated by a one-dimensional analysis, i.e., semi-infinite, slab, and spherically symmetric geometries. It is anticipated that this restriction will be removed after accumulating a body of experience with one-dimensional applications.

The computer program is not particularly long and it was deliberately constructed in a modular programming style; there are no subroutines in the

version given here as Appendix B. This method was chosen for several reasons. First, LASER8 breaks new ground in the numerical treatment of moving boundary problems and we expect the program to continue to evolve as it is applied more extensively. Secondly, we anticipate that the problems for which the program is used will fall as much into the area of fundamental research as in the area of engineering applications. As a consequence, the program was developed from the beginning in a different spirit than that of a program like HEATING5, which can treat many different geometries and combinations of materials but is based on overly restrictive assumptions about phase changes and does not address the question of nucleation. Finally, for problems involving complex state changes, very small finite-difference cells, long laser pulses, or various combinations of these factors, the running times can become quite long. (For a great variety of problems, however, LASER8 is simple enough and fast enough to program and run on a personal computer.) In order to reduce these times, certain segments of the program are "hardwired" for the material being studied and analytical fits to functions, rather than table look-up procedures, are used throughout. These restrictions can easily be removed if it appears desirable to do so.

In the next section we first describe two classes of experimental observations that illustrate the need for a program such as LASER8, we then review briefly classical solidification and nucleation theories, and lastly give an overview of the mathematical approach we found most useful in developing the program. In Section 3, a detailed description of the foundations of the modeling and our approach to its implementation are presented. In Section 4, an explanation is given of the manner in which changes of

phase and state, overheating and undercooling, and nucleation can be treated in the model. This explanation involves a detailed description of state diagrams and state arrays and examples of how they are constructed and used in the computer program. Section 5 contains discussions of several aspects of the numerical methods used, and illustrative results from the extensive testing of LASER8 are provided in Section 6. A few concluding remarks about various aspects of the work reported here are contained in Section 7. Applications of the modeling to systems other than elemental semiconductors are also briefly considered in this section. Appendix A is a guide to the use of one version of LASER8 and Appendix B is a program listing of that version. These Appendices are reasonably self-contained and a reader may find it useful to consult them frequently while reading Sections 3-5.

2.0 Experimental and Theoretical Background

2.1 Some Effects of High-Power Laser Pulses on Semiconductors

Pulsed laser processing of materials, especially semiconductors, is a field of condensed matter physics and materials science that has developed rapidly over the last few years.[1] It has proved to be of considerable interest for both applied and fundamental research for a variety of reasons discussed extensively in the literature.[5] We are most interested in it here because it provides for the first time a tool for well-controlled studies of physical processes occurring far from thermodynamic equilibrium; it was the results of such studies that stimulated the development of LASER8. To be more specific, radiation of semiconductors with nanosecond (10^{-9} sec)

and picosecond (10^{-12} sec) pulses from high-powered lasers can result in complex changes of the near-surface regions brought about by ultrarapid melting and solidification. There are two well-documented classes of observations in silicon that illustrate complementary aspects of the phase change and nucleation phenomena to be modeled by LASER8.

The first class demonstrates that when liquid (ℓ) silicon is caused to solidify in a 100 direction with a phase-front velocity of 15–20 m/sec (by a proper choice of laser pulse), the solid regrows in an amorphous (a) rather than crystalline (c) state.[6-8] There is good evidence that the melting temperature T_a of a-Si is ~200–300°C lower than T_c,[9] the melting point of c-Si. From a purely thermodynamic standpoint, the formation of a-Si from ℓ-Si would seem to imply that an undercooling of at least T_c-T_a has been achieved without nucleation and growth of the c-phase. Without delving into the details of classical phenomenological crystal growth theory, it should be apparant from this example that inclusion of liquid phase undercooling is essential in mathematically modeling the ultrarapid solidification involved in this example. In fact, interfacial undercooling of the liquid is required for solidification at any rate (see Sec. 2.2), but for most materials of interest here it is only at relatively high growth rates that the effects of undercooling become important.

The observation complementary to the foregoing one involves the pulsed laser melting of an a-Si layer, formed on a substrate by a variety of techniques, and the subsequent solidification of the ℓ-Si.[10-15] Since this is the situation used in describing the model developed here, we will consider the experimental results in somewhat more detail than for the preceding

case. The upper schematic illustration in Fig. 2.1 represents the initial condition of the sample; it consists of a c-Si substrate with an a-Si surface layer formed directly in the c-Si by, for example, ion implantation. When this a-Si layer is partially melted by a laser pulse, highly undercooled ℓ-Si is formed ($T \approx T_a$ at the interface between the a- and ℓ-Si). After such a pulse it is observed that two regions of polycrystalline silicon (p-Si) have been formed and the extent of these regions varies with the pulse energy density E_ℓ. For values of E_ℓ just above the threshold for melting of the a-Si, only a fine-grained (FG) p-Si is formed. As E_ℓ is increased, a region of large-grained (LG) p-Si begins to appear in the region nearest the surface, followed in succession by the FG material, the a-Si, and finally the c-Si substrate; this situation is indicated in the lower illustration of Fig. 2.1. As E_ℓ is increased still further, the LG region increases at the expense of the FG and amorphous regions until both

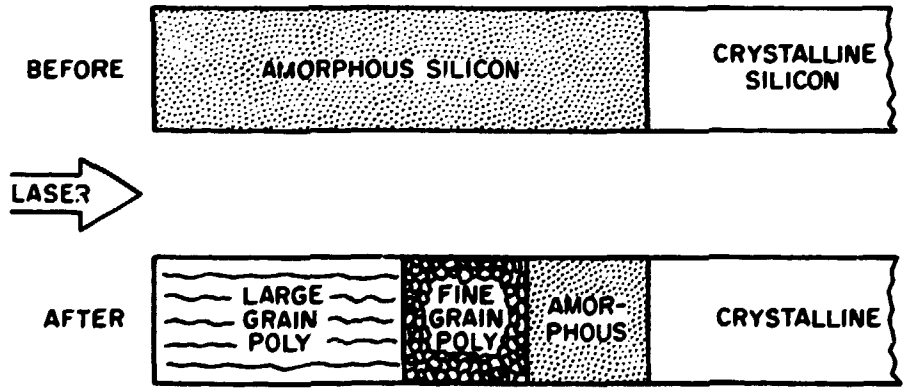

Fig. 2.1. Illustration of the morphological changes induced by pulsed laser irradiation of an a-Si overlayer on a c-Si substrate.

of these regions disappear altogether. At sufficiently high values of E_ℓ, the LG p-Si is no longer formed and only single crystal material is observed. The lowest energy density at which this occurs is interpreted as the E_ℓ required to melt through the a-c interface and produce liquid-phase epitaxy from the c-Si substrate; the c-Si formed in this way is virtually defect free. Further complicating this already complex behavior, is the recent observation[16] that in some instances large-scale three dimensional features may be superimposed on the essentially planar morphologies of Fig. 2.1.

We saw in the above two examples that large undercoolings of ℓ-Si are an important aspect of the solidification behavior of pulsed laser melted silicon. As already mentioned in the Introduction, one of the primary motivations for the work described here was to develop a method for including overheating and undercooling in the calculations. Also, as already noted, to adequately treat the many cases arising in practice it would seem necessary to include an approximate method for simulating nucleation events and their effects on the heat flow problem. Consider, for example, the case illustrated in Fig. 2.1 in which FG and LG p-Si are formed from undercooled ℓ-Si that is separated from the c-Si substrate by an a-Si layer. It is generally thought that nucleation of some form, heterogeneous or homogeneous bulk nucleation or nucleation at an interface, is required to explain the observation of a crystalline phase formed from a liquid phase completely embedded in an amorphous or glassy matrix. Provisions for simulation of nucleation phenomena have been incorporated into our modeling through the introduction of nucleation temperatures and timers, as described below.

2.2 Classical Crystal Growth Theory

The classical phenomenological theory of crystal growth[17-19] expresses the velocity of a liquid-solid interface as the difference between forward and reverse kinetic rate constants, i.e.,

$$v = K_f - K_r \ . \tag{2.1}$$

K_f is the rate (in velocity units) at which atoms leave the liquid and join the solid, while K_r is the rate for the reverse process. K_f and K_r are generally considered to represent activated processes and are expressed as

$$K_f = A_f \exp\left(-\Delta H^{\ell s} / kT\right) \tag{2.2}$$

$$K_r = A_r \exp\left(-\Delta H^{s\ell} / kT\right) \ . \tag{2.3}$$

$\Delta H^{\ell s}$ and $\Delta H^{s\ell}$ are the activation energies, defined by reference to Fig. 2.2, and T is the temperature. From Fig. 2.2 it can be seen that $\Delta H^{\ell s} - \Delta H^{s\ell}$ is L_c, the latent heat of crystallization per atom. By simple algebraic manipulation of Eqs. 2.1–2.3, an expression for the melt-front velocity can

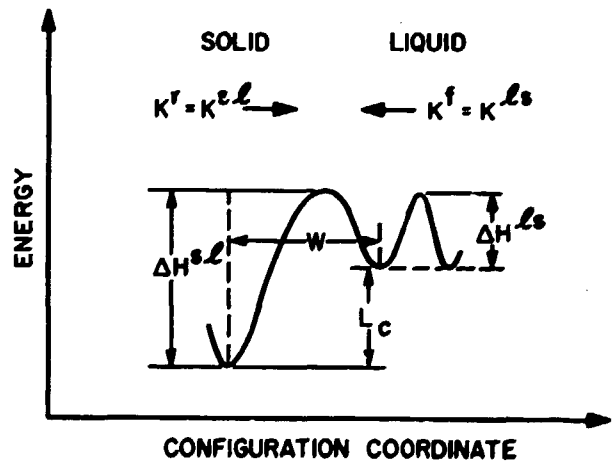

Fig. 2.2. Kinetic processes at the liquid-solid interface. L_c is the latent heat of crystallization. W is the width of the interfacial region.

be obtained in the form

$$v = K_f(T_i)\{1 - \exp(-(L_c/kT_c)(\Delta T_i/T_i))\} , \qquad (2.4)$$

in which T_c is the crystallization temperature, T_i is the "interface temperature", and the interfacial undercooling ΔT_i is given by $\Delta T_i = T_c - T_i$. The ratio of the pre-exponential factors in Eqs. 2.2 and 2.3 is fixed from the equilibrium condition that the phase interface (melt front) be stationary, i.e., $v = 0$. An expression such as Eq. 2.4 is important because it demonstrates that $\Delta T_i \neq 0$ is necessary for any motion of the interface and illustrates how the velocity of the melt front may depend on atomic processes in the interface region. In other words, this means that undercooling of the liquid is required for solidification and overheating of the solid for melting. Here we will be concerned primarily with undercooling, but the requirement of overheating for melting should be kept in mind.

From conventional heat conduction equations,[20] the velocity of a planar interface for crystallization can be obtained from the one-dimensional heat flux boundary condition at the liquid-solid interface, i.e.,

$$\frac{dQ}{dt} = A\rho L_c \frac{dx}{dt} = K_\ell[\text{grad } T]_{i,\ell} - K_s[\text{grad } T]_{i,s} . \qquad (2.5)$$

The product Adx is the volume of material changing phase in time dt, ρ is the density, K_ℓ and K_s are the thermal conductivities in the liquid and solid respectively, and the notation indicates that the gradients of T in the liquid and solid are to be evaluated at the interface. It is usually assumed in calculating the gradients that the interface is at the thermodynamic phase change temperature T_c. This assumption together with Eq. 2.5 and the heat diffusion equation (see Sec. 3.2) are frequently referred to as the Stefan problem.[21-22] We note again that if the interface temperature

were actually T_c, ΔT_i in Eq. 2.4 would be zero and there would be no movement of the phase front. For small values of ΔT_i and large temperature gradients, the errors made in calculating the gradients as though the interface were at T_c should be very small, and the velocity of the interface given quite accurately by Eq. 2.5. If ΔT_i becomes large, this may no longer be the case, particularly because of the activated rate constant appearing in Eq. 2.4. It will then be necessary to explicitly introduce interfacial undercooling effects into the calculations; this is precisely one of the problems LASER8 was designed to address although a discussion of it will be deferred to a later publication. If the motion of the melt front is controlled by Eq. 2.5 it is said to be heat-flow limited and if it is controlled by Eq. 2.4, it is said to be limited by the interfacial kinetics.

2.3 Phenomenological Nucleation Theory

Nucleation theory[17,23,24] deals with the problem of how a new phase begins to form in a material not initially containing that phase. We will assume that some type of nucleation event must occur in order to initiate growth of small nuclei, sometimes called embryos, of the new phase. The nucleation events may occur at free surfaces or interfaces, at impurities or impurity aggregates, or they may occur homogeneously in the bulk of the pure material through statistical fluctuations. In the case of amorphous materials formed by ion implantation, sputtering, or electron beam evaporation, it is possible that minute inclusions of crystalline material are embedded in the amorphous phase.

Although most metallurgists apparently feel that true homogeneous bulk nucleation is rare, a simplified theory of it will be sketched here to illustrate the general ideas involved in phenomenological nucleation theories.

To be specific, let us assume that a molten material, totally devoid of impurities, is enclosed in a container with which it has no interactions that will themselves serve to nucleate a phase change. As the temperature of the liquid is lowered below the thermodynamic phase change temperature, the liquid phase becomes metastable relative to the solid phases. At any given undercooling, clusters of atoms may begin to form into solid-like configurations. However, these clusters will generally be unstable because the surface energy of the phase interface is greater than the energy gained by formation of the more stable solid phase. Stated another way, the liquid is constantly undergoing local fluctuations from the liquid to the solid state, but the probability that the fluctuations will result in solid nuclei large enough to be stable and to begin to grow is exceedingly small. As the temperature is lowered still further the size of a critical nucleus becomes small enough and the fluctuations large enough that stable nuclei can form and grow. The nucleation rate then increases so rapidly over a small temperature range that it is a good approximation to speak of a *nucleation temperature*.

The foregoing can be stated more quantitatively for spherical nuclei as follows. For a nucleus of radius r the change of free energy associated with the formation of the nucleus is given by

$$\Delta G = 4\pi r^2\sigma + 4\pi r^3\Delta G_V/3 \ , \qquad (2.6)$$

in which σ and ΔG_V are the surface and volume free energies, respectively.

Setting $d\Delta G/dr = 0$ gives

$$r^* = -2\sigma/\Delta G_V \ , \quad n^* = 4\pi r^{*3} N_V/3 \tag{2.7a}$$

and

$$\Delta G^* = 16\pi\sigma^3/3(\Delta G_V)^2 \ . \tag{2.7b}$$

r^* is radius of the critical nucleus in the undercooled liquid, n^* is the number of atoms in it, and N_V is the number of atoms per unit volume. If the difference in heat capacity between the liquid and crystalline solid can be neglected, ΔG_V can be expressed in terms of the interfacial undercooling as

$$\Delta G_V = -L_C \Delta T_i / T_C \ . \tag{2.8}$$

The surface free energy is seldom known accurately, which makes it difficult to estimate ΔG^*. For our purposes, however, it is sufficient to recognize that ΔG^* is the free energy barrier that must be surmounted for a nuclei to reach critical size and begin to grow. The temperature at which this occurs can be referred to as the nucleation temperature, T_n.

The nucleation rate is given in terms of ΔG^* by

$$I = I_0 \exp(-\Delta G^*/kT_i) \ , \tag{2.9}$$

in which I_0 has the units of $cm^{-3}\ s^{-1}$. The nucleation rate may be a difficult quantity to determine experimentally if it is high because of lack of time resolution in the experiments. Again, however, from the standpoint of our present goal of roughly simulating nucleation processes, it is enough to recognize that a nucleation temperature and rate, or a time if we deal with the reciprocal of I in Eq. 2.9, can be used in the simulations.

It is apparent from the foregoing discussion that nucleation events are likely to be two and three dimensional processes and we must be concerned about how they can be simulated in a one-dimensional calculation. Frequently it may be that this can only be done in some quite approximate way. We will discuss this later after the finite-difference equations have been introduced.

2.4 Mathematical Approach

A variety of methods for treating moving boundary problems was investigated during the course of the development of LASER8.[25] We sought a method that would enable us to study the physical problems discussed above and that would serve as a basis for a flexible and efficient finite-difference, or finite-element,[26] computer program. A method apparently first developed by Rose[27,28] was finally chosen. As discussed in the next section, this method emphasizes the fundamental role of enthalpy in a phase change process and uses the temperature simply to determine the heat fluxes. This has the advantage that the determination of a phase or a state of a small volume of material is based on its enthalpy content rather than its temperature. Thus, a phase change can occur, in principle, at any temperature, with the result that overheating and undercooling can be included in the formalism. A relationship between the extent of overheating or undercooling and the velocity of the phase interface must be specified as a boundary condition (see the discussion in Sec. 2.2), but this condition need not be restricted to the commonly used requirement that the phase change occur at the equilibrium thermodynamic melting temperature. For the same reason, nucleation

effects can be treated because a material can be overheated or undercooled to a prescribed nucleation temperature and held there for a prescribed time before the latent heat of the nucleating phase comes into play. To realize the full flexibility of this method, the various changes of phase and state, and the conditions under which they can occur, can be specified by a state array. The only fundamental restriction on the state array is that all of the processes involved must conserve energy. This will be illustrated in detail in Sec. 4.

3.0 Model for Heat Transfer and State Change

3.1 General Assumptions

The laser-irradiated sample is modeled as either a slab or a semi-infinite solid extending in the positive x-direction and composed of up to nine layers, each of arbitrary but uniform thickness. The laser pulse is assumed 1) to have a cross section large compared to the depth into the sample for which significant temperature rises occur and 2) to be homogeneous in energy across any y-z plane. In practice, condition 1) is easily realized and, with care, 2) can probably be approximated adequately although complete homogeneity is basically unattainable. As a result of these conditions, the laser annealing process can be treated as a one-dimensional problem, provided that any nucleation effects to be included can be simulated within the framework of a one-dimensional approximation. As already mentioned, this will be discussed in more detail below.

The optical and thermal properties of the individual layers of the sample may be functions of temperature, phase, and state. For example, with reference to the case illustrated in Fig. 1.1, it is well known that the materials properties of a-, c-, and ℓ-Si are quite different (see Fig. 5.1 for the thermal conductivity of a-, c-, and ℓ-Si), but it is also likely that a property such as the thermal conductivity of polycrystalline silicon depends on the grain size and orientation. Provisions for handling these differing properties are incorporated into the computer program, but it is often difficult to know reliable values of the input data for a complex state.

The left boundary, i.e. the surface at $x = 0$, is assumed to be insulated. Calculations have shown that this is a good approximation for laser pulses of nanosecond and picosecond duration because the times involved are too short for convection or radiation losses[4] to be important. Should convection and radiation losses become important for long duration pulses, they can easily be incorporated into the model. If the sample is semi-infinite, the temperature of the right boundary is assumed to remain constant at its initial value throughout a calculation. Calculations for a finite slab may require other boundary conditions. The way in which the right boundary is actually treated in the finite-difference calculations is described in Sec. 5.1.

3.2 Enthalpy Form of the Heat Flow Problem

It has been customary in the past in the vast majority of treatments of heat flow problems to maintain the temperature distribution $T(x,t)$ in

the sample at the focus of attention. In the laser irradiation case, this leads to the usual partial differential equation for T(x,t) with the expression for the energy in the laser pulse providing a source, or heat generation, term.[4] We have not found this a convenient method for dealing with problems in which phase changes can occur at temperatures that may vary during the problem, e.g., when undercooling must be taken into account. Instead, we have employed the above-mentioned method developed by Rose, which is based on an enthalpy formulation of heat flow.[29] Although it is straightforward to convert the differential equation for T(x,t) into an equation for the enthalpy, for completeness and to remind the reader of some of the approximations involved, we will derive the enthalpy equation directly from the usual energy balance condition. In integral form this condition is given by

$$\frac{d}{dt}\int_V \rho e dv = \int_V S dv + \int_A K\nabla T \cdot \vec{n} da = 0, \tag{3.1}$$

in which ρ is the density, e the internal energy, and K the thermal conductivity in a given differential volume element dv. S is the heat generation function describing the effects of the laser pulse and $\vec{n}$ is an outwardly directed unit vector normal to the element of area da. The left hand side of Eq. 3.1 is the rate of change of the energy stored in the volume V, the first term on the right hand side is the rate at which energy is generated by the laser pulse and the second term is the rate of change of stored energy due to conduction into and out of A, the surface bounding V. The heat balance equation at any time is illustrated schematically in Fig. 3.1.

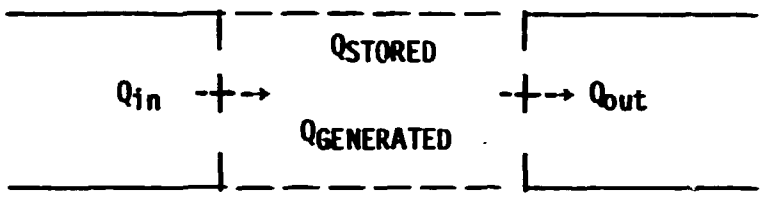

Fig. 3.1. Schematic illustration of heat balance in a small volume of material.

The enthalpy h is related to the internal energy and the pressure p by the equation

$$e = h - p/\rho, \tag{3.2}$$

which when substituted in Eq. 1 gives

$$\frac{d}{dt}\int_V [\rho h - p]dv = \int_V S dv + \int_A K\nabla T \cdot \vec{n} da \ . \tag{3.3}$$

The pressure is generally assumed to be independent of time during a phase change[30] (isobaric process) and Eq. 3.3 then becomes

$$\frac{d}{dt}\int_V \rho h dv = \int_V S dv + \int_A K\nabla T \cdot \vec{n} da. \tag{3.4}$$

Application of the divergence theorem to the second term on the right hand side and interchange of the order of integration and differentiation yields

$$\int_V \frac{\partial}{\partial t}(\rho h)dv = \int_V S dv + \int_V \nabla \cdot (K\nabla T)dv \tag{3.5}$$

Since Eq. 3.5 is true for any volume element, we finally obtain the enthalpy equation

$$\frac{\partial}{\partial t}(\rho h) = \nabla \cdot (K\nabla T) + S. \tag{3.6}$$

In one dimension this becomes

$$\frac{\partial}{\partial t}(\rho h) = \frac{\partial}{\partial x}\left(K \frac{\partial T}{\partial x}\right) + S \ , \tag{3.7}$$

which is the starting point for the LASER8 discretization. One further simplification is often possible because ρ is very nearly independent of temperature and phase for many materials, e.g. silicon, and hence does not change with time.

3.3 Source Term

The absorption of energy from the laser pulse and the conversion of this energy into heat provide the source term, represented by S in Eq. 3.7, in the problem. This term can become very complicated and a detailed treatment of it here would be inappropriate. Instead, we will provide a simple illustrative treatment that is valid for many cases and then briefly indicate some of the complexities that may arise.

Because the penetration depth of the laser radiation may be comparable to the region over which significant temperature changes occur, it is not accurate to assume that the laser pulse can be represented simply by a flux term at the surface of the slab. In order to model the absorption of the laser pulse accurately, the source term must be made a function of depth as well as time. For a constant absorption coefficient α (linear regime), the absorption of light by a solid or liquid follows an exponential law. In such a case, the amount of energy penetrating to a particular depth at time t can be approximated by

$$S(x,t) = (1 - R(x,t))\, P(t)\alpha e^{-\alpha x}. \qquad (3.8)$$

where R(x,t) is the reflectivity of the sample and P(t) gives the variation in intensity of the laser pulse with time. Reflection of light from a

material is not a purely surface phenomena and can therefore depend on both x and t, primarily because of the change in temperature and phase with x and t. For simplicity, we assume that R is a function only of the temperature and phase of the surface finite-difference cell. The separation of the absorption function into a product of time-dependent and x-dependent factors will also not be discussed. P(t) is often very nearly a gaussian for solid state lasers, but can have complex forms for gas lasers. A typical excimer laser pulse shape is shown in Fig. 3.2. Although the sharp structure on this pulse need not be duplicated, the overall shape should be reproduced resonably well. In order to determine the amount of energy that is deposited in a finite region of the slab, the factor $\alpha \exp(-\alpha x)$ in Eq. 3.8 can be integrated to obtain

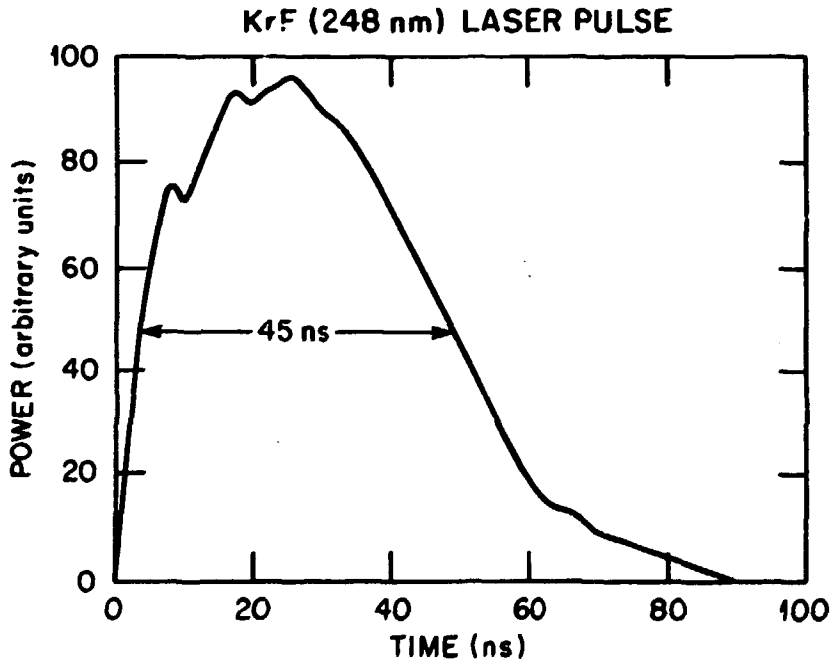

Fig. 3.2. The time dependence of a typical excimer laser pulse.

$$\int_{x_1}^{x_2} \alpha e^{-\alpha x}\, dx = -e^{-\alpha x}\Big|_{x_1}^{x_2} . \tag{3.9}$$

This expression when substituted back into Eq. 3.8 leads to a very simple analytical relation for determining the internal heat generation rate in any finite-difference cell of the sample.

It may happen that the absorption coefficient α is not constant and then the simple treatment given here no longer holds. It is not difficult to include temperature- and intensity-dependent (nonlinear) absorption in the modeling but this has not been implemented in the present version of LASER8 because the values of α for the laser radiation used in the experiments modeled to date are so high ($> 10^6$ cm^{-1}) that these effects are unimportant. For long-wavelength radiation, such as that from a CO_2 laser, α for a semiconductor can be expected to be a complex function of doping concentration, temperature, radiation-induced free carriers, carrier diffusion, etc. In such cases, separate routines for the calculation of α and R(x,t) may be usefully introduced.

3.4 Discretization

Equation 3.7 was discretized using the classical forward time difference scheme. This gives an explicit method for updating the enthalpies from time step n to n + 1. For the i-th cell in the bulk of the material the finite difference equation becomes

$$\rho \frac{h_i^{n+1} - h_i^n}{\Delta t} = \frac{1}{\Delta x^2} \frac{K_{i+1}+K_i}{2}(T_{i+1}^n - T_i^n) + \frac{K_i+K_{i-1}}{2}(T_{i-1}^n - T_i^n) + S_i^n . \tag{3.10}$$

It should be noted that the effective thermal conductivity for heat conduction between cells i and i+1 is given as an average of the conductivity in the two cells. The question of how to treat the conductivity of a cell that is partially solid and partially liquid is discussed in Sec. 5.3.

The boundary cells must be handled differently from bulk cells. The cell at the surface will be discussed here and the one at the back boundary in Section 5. Since the surface is assumed to be insulated in the present version of LASER8, the appropriate boundary conditions on the temperature and energy profiles can be obtained by reflection of these profiles in the plane of the surface. The second order discretization scheme can then be preserved if the surface cell is assumed to be half as wide as a bulk cell and the method of images is used. Thus, the equation for the surface node becomes,

$$\rho \frac{h_1^{n+1} - h_1^n}{\Delta t} = 2\frac{K_1+K_2}{\Delta x^2} (T_2^n - T_1^n) + S_1^n \qquad (3.11)$$

There were two main reasons why a more complex discretization scheme (for example Crank-Nicholson) was not used. First, the intensity of the source term is often so large and changing so rapidly that small time steps are generally required to describe it. The intensity of the laser pulse may also cause the melt front to move at very high velocities (as high as 100 m/s). The advantage of using higher order schemes is that they typically allow much larger time steps at the cost of computational effort. Since in most of the cases of interest here the time step must be small to track the front accurately and model the laser pulse satisfactorily this

advantage is lost. Second, state arrays are set up on the assumption that only one change of phase can occur in a time step. This is a reasonable assumption only if the time step is small. If a large time step were used, more than one path through the state array might yield an energy balance, thus leading to a lack of uniqueness in the solution. Again since a small time step is needed to model the problem with sufficient accuracy, the explicit finite-difference scheme proved computationally more efficient than more complex schemes.

3.5 Simulation of Nucleation

We now turn to a brief discussion of the extent to which two- and three-dimensional nucleation events can be simulated in a one-dimensional calculation. We assume that a nucleation event releases latent heat and rapidly raises the temperature of the just-formed embryo to some temperature greater than that of the surrounding undercooled liquid; for convenience let us assume that this temperature is T_c, the melting temperature of the crystalline material. If the undercooling is large, very large temperature gradients will be set up and the flow of heat from the growing nuclei may be very rapid, depending on the thermal conductivity of the liquid. If many nucleation events occur in close proximity to one another and more or less simultaneously, the temperature of an extended region will be raised nearly uniformly. The composition of the material in this region will be a mixture of solid and liquid (referred to as "slush" in the next section). As the heat is conducted away from this region, the nuclei will continue to grow until the material completely solidifies.

Now assume that a planar phase interface, separating an undercooled liquid such as ℓ-Si and a solid such as a-Si, is present. The thermal conductivity of ℓ-Si is an order of magnitude or more greater than that of a-Si. Suppose that a nucleation event occurs at or near this interface. The heat liberated will flow rapidly into the liquid and much less rapidly into the solid. Again, if the density of nucleation events occurring nearly simultaneously is high, the temperature of the ℓ-Si will be raised more or less uniformly and the planar interface approximately preserved. Rapid liquid phase epitaxial regrowth can be thought of as a limiting case of this type of situation. Every lattice site is a potential nucleation site and, at least for a rapidly moving interface where step growth is relatively unimportant, the nucleation events over the interface occur virtually simultaneously; in this case a one-dimensional calculation would seem to be justified.

In view of the above discussion, we conclude that the density and frequency of nucleation events, the volume to which they are confined, and the relative magnitude of the liquid and solid thermal conductivities will be important in determining the adequacy of a one-dimensional calculation. Unfortunately, it is unlikely that reliable information about nucleation processes in a given situation will be available. We must then rely on the experimental results and the agreement between these and results of model calculations to establish the adequacy of a one-dimensional calculation, ex post facto.

4.0 State Diagrams and Arrays

We have discussed above the general assumptions of our model, the boundary conditions, and the discretization scheme. We now turn to the two most important innovations of our approach. In order to cope with the complexeties of the problems we wish to address, it is necessary to have a scheme in which the material in each finite-difference cell can change its phase or its state in accordance with a set of prescribed conditions and subject only to the requirement of energy conversation. In order to accomplish this, we have introduced the state diagram and the state array which are discussed in this section, together with the interpretation of the mixed two-phase state referred to as "slush".

4.1 The State Diagram

Figure 4.1 gives a form of the entire state diagram for the case of silicon, while Fig. 4.2 shows a schematic of the region in the neighborhood of the liquid-solid transitions on an expanded scale. The state diagram is drawn in a manner that reflects our emphasis on enthalpy as the most useful thermodynamic quantity. We note here that a horizontal line on the state diagram corresponds to the evolution of latent heat at constant temperature, and therefore to a first order phase change. There is good evidence that a-Si, unlike true glasses, undergoes a first order phase change on melting and solidifying. Let us consider several examples of a succession of changes and transformations that may occur in a small volume element of material subjected to heating and cooling.

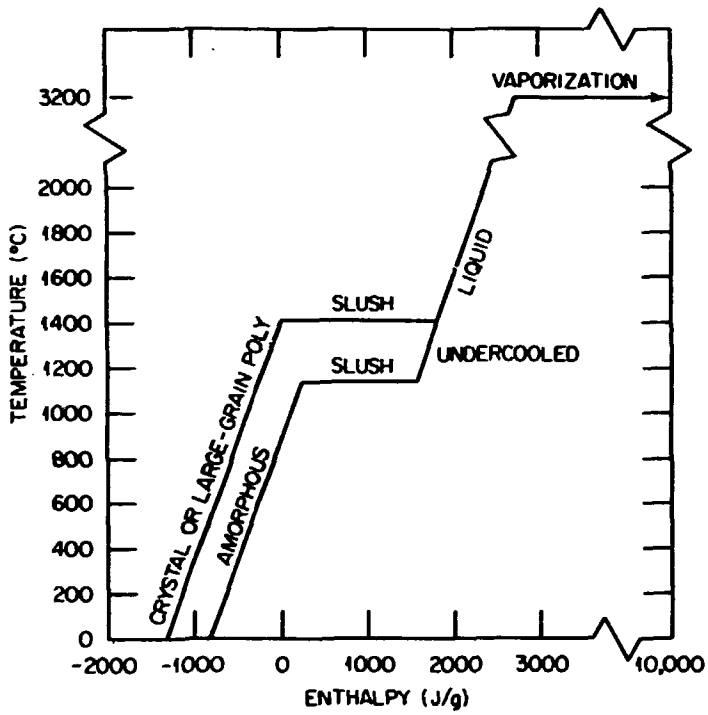

Fig. 4.1. State diagram for silicon. The zero of enthalpy is taken as that of the crystalline material at the melting point of c-Si.

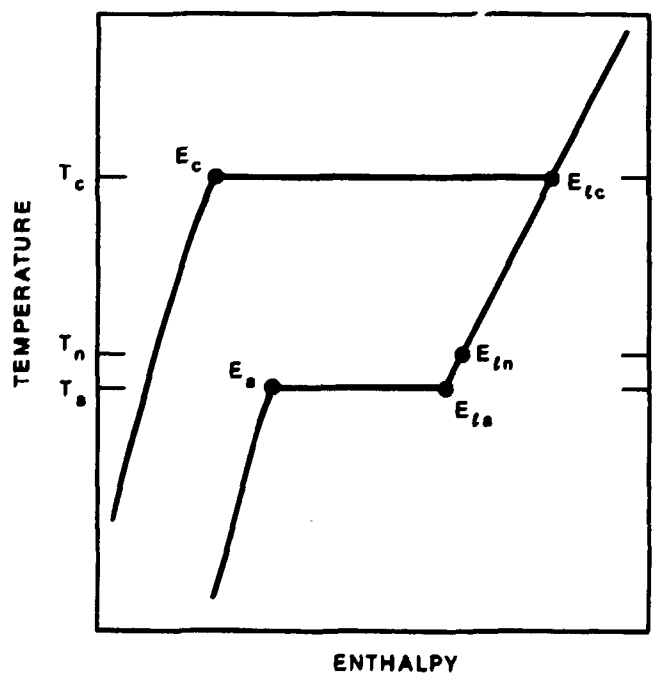

Fig. 4.2. State diagram for silicon in the neighborhood of the solid-liquid phase transition or an expanded scale.

In the first example, we assume the material to be initially c-Si and to be subjected to slow heating and cooling. As the sample is heated, the temperature and enthalpy increase along the line labeled "crystal or large-grain poly" on Fig. 4.1 until E_c and T_c on Fig. 4.2 are reached. The material undergoes melting along the line marked "slush," with the temperature remaining constant at T_c, while the enthalpy changes until enough latent heat is absorbed to completely melt the volume of material under consideration. At $E_{\ell c}$ on Fig. 4.2 the temperature of the liquid begins to increase again with increasing enthalpy and continues to do so until the vaporization line is reached. If at some time after melting but before vaporization the material is allowed to cool, the temperature falls until $E_{\ell c}$ and T_c are reached. When, as we have assumed, the cooling rate is small, so that there is little undercooling, and there is crystalline material contiguous to the material under consideration, the system will very nearly reverse its heating path. This would correspond to near-equilibrium epitaxial growth either from a crystalline substrate or from already formed crystallites in polycrystalline material.

Suppose, however, that the liquid is completely isolated from any solid material that could serve as a template for epitaxial crystal growth. Then the liquid may sustain large undercoolings until some nucleation event occurs to initiate crystalline growth or until the system reaches $E_{\ell a}$ and amorphous material forms at T_a. In fact, it may be possible that such a system could be further undercooled to some other state resembling a true glassy material. We will not consider this possibility here, although it could be incorporated into the modeling without difficulty. If no nucleation

event occurs, Fig. 4.2 suggests that the system will return as a-Si. To our knowledge, a-Si has never been formed by slow cooling from the liquid state but the possibility cannot be ruled out. The more common observation is that polycrystalline Si is formed, triggered presumably by some nucleation event. The nucleation may occur in the bulk or at an interface, as discussed in Sec. 2.3.

Returning now to our state diagram, we must consider what happens when a nucleation event occurs. A precise answer to this is very difficult, and probably not known in most cases of interest. In the present modeling we have assumed that when nucleation occurs, the temperature of the solid embryo is suddenly raised to T_c because of the release of latent heat. Although this may seem like a reasonable assumption, it is probably in fact an oversimplification since the kinetics of the nucleation process and the thermal conductivity will govern the release of latent heat and its rate of diffusion into the surrounding liquid. In other words, the growth of an embryo will probably be interface limited. Moreover, the difficulty in treating nucleation is compounded by the fact that it is essentially a three dimensional process and we are trying to simulate its effects in a one-dimensional, finite-difference calculation. If the density of nucleation events is sufficiently high that three-dimensional effects occur only over spatial regions small compared to the cell size of the finite-difference calculations, a one-dimensional treatment can probably be justified, as discussed in Sec. 4.2. In any case, it is assumed here that when a nucleation event occurs in a given cell the temperature of the entire cell is raised to T_c by a vertical transition from the $E_{\ell a}$-$E_{\ell n}$ line to the E_c-$E_{\ell c}$

line. Such a transition is guaranteed to conserve energy. The quantities $E_{\ell n}$ and T_n appearing on Fig. 4.2 are nucleation enthalpies and temperatures. They are utilized in the modeling as follows. If the system (i.e., in practice a finite-difference cell) is undercooled to temperatures in the range from T_a to T_n and remains there for a time t_n, a nucleation event can occur, provided certain other conditions specified by the state array are satisfied.

Our second illustration of the use of the state diagram deals with the situation shown in Fig. 1.1, i.e., melting of an a-Si layer and resolidification on a c-Si substrate. In this case the enthalpy and temperature increase along the "amorphous" line of Fig. 4.1 until E_a and T_a in Fig. 4.2 are reached. The a-Si then begins to melt along the line E_a-$E_{\ell a}$ with the temperature remaining constant. At $E_{\ell a}$ the material is fully molten but highly undercooled. If the temperature remains between T_a and T_n long enough for nucleation to occur, transitions to the E_c-$E_{\ell c}$ line will be made as described in the preceding example. If the line segment $E_{\ell a}$-$E_{\ell n}$ is traversed rapidly enough, nucleation will be suppressed although the liquid may still be undercooled. For high enough energy input from the laser, the liquid will be heated to $T > T_c$. On cooling a variety of events can occur, depending on the conditions specified in the state array discussed in Sec. 4.3.

Our final example deals with the case mentioned in subsection 2.1 in which solidification is so rapid that material that was crystalline before melting is found to be amorphous on solidifying. For simplicity, we assume that the melting part of the process follows the same path as that for the

first case considered. On cooling, however, we assume that when the velocity of the melt front reaches some critical value v_a, the liquid does not have time to form a crystalline solid and instead makes a transition to the amorphous phase. Since such high velocities imply large undercoolings, it is again necessary to treat the undercooling in some detail. However, it is apparent that both the magnitude and the rate of undercooling are important. For example, adhering strictly to the diagram on Fig. 4.2, it would appear that the material must traverse the line $E_{\ell n}$-$E_{\ell a}$ in a time less that t_n so that nucleation can be suppressed if a-Si is to be formed.

4.2 Transition States, Mushy Zones, and Slush

As mentioned above, the state diagram of Fig. 4.1 shows a segment labeled "slush". In this subsection we elaborate on this terminology and its meaning.

From the standpoint of a finite difference calculation, any particular cell is said to be undergoing a transition when the material in the cell is changing from one state to another; the most common transition will be between the solid and liquid states. The liquid (or solid) fraction in a given cell will be determined by the amount of latent heat given up at any time relative to the total amount of latent heat involved in the phase change. More specifically, the transition ratio can be defined as the ratio of heat which has been absorbed or liberated after the transition temperature has been reached to the total heat needed to complete the phase change for a material in a given cell. The transition ratio says nothing about the location of the phase front in the cell, and to locate such a

front within a cell additional assumptions have to be made, as discussed in the next section. If several contiguous cells are undergoing transitions at the same time, the position of a phase front cannot be defined on the spatial scale of the finite-difference calculation. The material in these cells can then be envisioned as in a "mushy" state frequently referred to as "slush". Although this terminology is not elegant, it is descriptive and it is often encountered in the literature[31] in various contexts related to the one discussed here (e.g., the growth of dendrites into undercooled liquids).

The discussion above seems to suggest that we should think of the slush state on Fig. 4.1 more as an artifact of the finite-difference formulation than as a true physical state. In those cases where there is a well-defined phase front with an interfacial region much smaller than the width of the finite difference cell in which it is located, it is clear that reference to the whole cell as being in a mushy state is an outgrowth of the finite-difference formulation. In those cases in which many cells are undergoing transitions more or less simultaneously, it seems likely that these cells constitute an extended zone in which a two-phase mixed state resembling ice-water slush actually exists. An unlikely alternative to this interpretation would be to assume that the entire extended region constitutes an interfacial region in which the properties of the material are changing from those of one phase to those of another uniformly. In any case, we believe it is appropriate to classify slush or mush as a distinct state on the state diagram.

We should point out in connection with this discussion, that homogeneous or heterogeneous bulk nucleation over regions of only a few finite difference cells should also lead to the formation of extended slush zones consisting of the nucleated solid material embedded in the undercooled liquid. These effects are easily identifiable in some of the modeling that has been done with LASER8.

4.3 State Arrays

LASER8 has the capability of treating many different phases and states simultaneously. In fact, the only fundamental requirement for a given finite-difference cell is that at any instant its state must be specified by the equation of state, or in other words, its temperature and enthalpy must correspond to a point on the curves of the state diagram. The time evolution of the state of a cell is determined by transitions between points on the curves of the state diagram. We have found it convenient to summarize the conditions under which a transition can be made from one state to another in the form of a state array. This array is used only for bookkeeping and is not involved in any algebraic manipulations; its implementation in the computer program is by way of a computed branching statement.

Figure 4.3 gives the simplest non-trivial form of a state array. It would be appropriate for the case in which only melting and crystallization of a single material, e.g., c-Si, is considered and overheating and undercooling effects can be neglected. This is the Stefan problem treated so often in the literature and already referred to above (see Refs. 21 and 22).

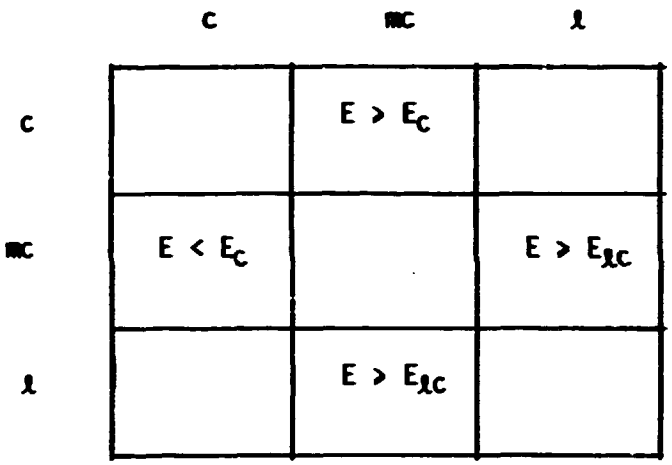

Fig. 4.3. State array for simple case of melting and crystallization. c - crystalline; mc - mushy crystalline; ℓ - liquid

Let us consider the elements of this array and how a given cell is transformed from one state to another. The diagonal elements of the array are blank because they represent no change of state. The (c, ℓ) and (ℓ, c) elements are blank because all transitions between solid and liquid states must go through an intermediate mushy state as the melt front moves through a cell. The melting and subsequent crystallization process is given by the sequence c → mc → ℓ → mc → c. Because of the simplicity of this problem the conditions making up the array elements depend only on the enthalpy and it is not necessary to specify the state of neighboring cells, values of nucleation timers, etc.

Figure 4.4 shows a version of the very complicated state array used in setting up LASER8 for studies of the situation depicted in Fig. 2.1. This version is used here only for illustrative purposes and is not necessarily the one most appropriate for reproducing the experimental results

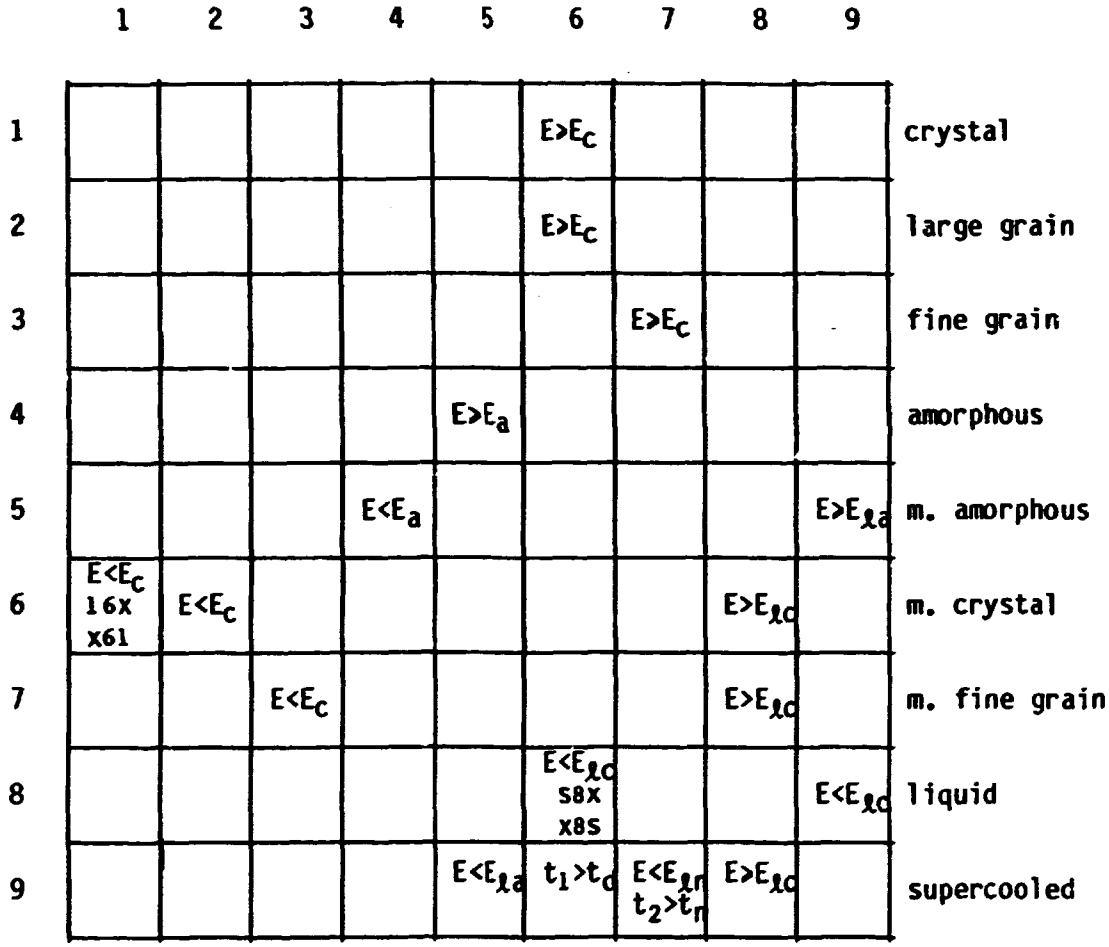

Fig. 4.4. One version of the state array for the melting and resolidification of an a-Si layer on a c-Si substrate. The labels on the right-hand side provide the correspondence with the numbering scheme of the array elements; m. stands for "mushy." t_1 and t_2 represent timers contained in the computer program. See the text for further details of the notation.

that have been obtained for melting of a-Si overlayers. Determination of the proper form of the state array for a complex problem can itself become a research undertaking. It should be noted that the state array contains a state labeled "m. fine grain". We found it useful to explicitly introduce such a state even though its latent heat and transition temperatures were assumed to be the same as those for mushy c-Si. In the same way, a mushy LG p-Si state could have been introduced but we did not find this useful. The physical significance of mushy zones has already been discussed in Section 4.2 and will not be considered further here. From a strictly programming standpoint they always appear as precursors to their solid state counterparts because the material in a finite-difference cell cannot change from a liquid to a solid state instantaneously (or more precisely in one time step). We will also consider a few of the elements of this state array and examples of how a cell can be transformed from one state to another.

The first example is a very simple one involving melting of the c-state. When the enthalpy of a given cell is increased to $> E_c$ the material makes a transition to a mushy crystalline state, as indicated by the (1,6) element in the state array. If the enthalpy continues to increase until $E > E_{\ell c}$, the cell makes a transition to the normal liquid state with $T > T_c$; this transition is given by the (6,8) element of the array. If there were no amorphous layer present and overheating and undercooling effects were negligible, melting and subsequent solidification on cooling would follow the path $1 \rightarrow 6 \rightarrow 8 \rightarrow 6 \rightarrow 1$. The (8,6) and (6,1) elements of the array give the conditions on the enthalpy for the indicated transitions to occur, but they also show that certain other conditions involving neighboring cells must be satisfied in more general cases.

First let us introduce a notational form to help in specifying these conditions. The general form employed consists of a sequence of three letters abc and means the following: the cell under consideration is the b cell and it can in principle be assigned any state number, the cell immediately to its left is the one nearer the surface and is labeled a, the deeper lying neighbor of b is the c cell. When a or c can be any state they are assigned the value x. If a neighboring cell is solid but the form of the solid is unimportant, a and c are assigned the letter s. If a neighboring cell is liquid but it is unimportant whether the liquid is normal or undercooled, a and c are assigned the letter ℓ. In all other cases, a state index number will indicate the condition of cells a and c.

Let us now consider the (8,6) element further. The appearance of the notation s8x means that the b cell (the cell under consideration) is in a liquid state, its neighbor to the left is solid, and the state of the neighbor to its right need not be specified. If these conditions are satisfied, the cell can make a transition to mushy crystalline material. However, the cell can also make the same transition if the states of a and c are interchanged. In either case the b cell is now in a mushy crystalline state and can make a transition to crystalline (6,1), LG polycrystalline (6,2), or FG polycrystalline (6,3) if the enthalpy drops below E_c. If the enthalpy of the cell increases to above $E_{\ell c}$ due to additional energy input from the laser pulse or from the release of latent heat in other cells, the b cell can remelt.

In the second example we will consider the conditions for each of the transitions that a supercooled liquid cell can undergo according to Fig. 4.4. These conditions are all on row 9 of the array. The (9,5) element requires that the change from supercooled liquid to mushy a-Si occurs when the enthalpy of the cell falls below $E_{\ell a}$, the minimum enthalpy that a cell can have and still be entirely liquid. The second possible change, given by (9,6), is from supercooled ℓ-Si to mushy c-Si. For this to occur a timer (TIMER1 in the program listing of Appendix B) must be greater than t_d, a specified nucleation or growth delay. This delay can be thought of as the time it takes for solidification of a supercooled liquid from an imperfect crystalline (e.g., a FG p-Si) interface to become established in a preferred growth direction; it is associated with the interface kinetics. TIMER1 keeps track of how long a supercooled cell has a neighboring cell that is either crystal, large-grained polycrystalline, or fine-grained polycrystalline. This state array assumes that nucleation and growth of a crystalline phase cannot occur off an amorphous interface. (The justification of such an assumption has not been clearly established.) The third transition (9,7) is from supercooled liquid to mushy FG material. This was assumed to be the path taken when the liquid nucleates. Two conditions must be met. First, the enthalpy must be less than E_n, the enthalpy above which bulk nucleation is improbable, and secondly a timer (TIMER2 in the program listing) must be greater than t_n, the specified nucleation time. Physically it is the time it takes for a nucleus of critical diameter to form within a cell undercooled below T_n. Finally, element (9,8) indicates that supercooled liquid can change to normal liquid. This occurs when the temperature of the liquid

equals or exceeds the melt temperature of the crystalline state. The condition for the change is that the enthalpy of the cell must exceed $E_{\ell c}$, the minimum enthalpy for which normal liquid material can exist.

5.0 Numerical Methods

In this section we discuss several aspects of the numerical methods used in LASER8. Additional information about these methods can be found in Appendix A and by studying the program listing in Appendix B.

5.1 Dynamic Rezone

Two forms of grid expansion are employed in LASER8. There is an initial growth of the mesh which follows the energy diffusion into the material, and then there is a buffer region added to the deepest part of the mesh to approximate a semi-infinite slab. With the exception of the buffer region all the nodes are equally spaced on the grid. This facilitated the coding and perserves the order of accuracy for the scheme. Grid expansion is done in the following way. Initially N nodes spaced ΔX apart are laid down starting at the surface. This mesh need not extend deeper than the depth the laser radiation penetrates into the slab. As the problem progresses the enthalpy of each of the nodes changes, and in particular the enthalpy of the N-1 node may exceed some small value ΔE above the ambient value. When this occurs a new node of width ΔX is added to the grid at ambient conditions, and N is incremented accordingly. When the enthalpy of the new N-1 node exceeds ΔE, another node is added and the process repeats itself

until N equals NMAX, the maximum number of nodes specified. NMAX should be large enough to extend the mesh well beyond the anticipated maximum melt-front penetration. This type of expansion of the equally spaced grid is completed when NMAX is reached and the second type of expansion is initiated, as described next.

Once the grid has been expanded to its initially defined maximum value, NMAX, and the NMAX-1 nodal enthalpy has exceeded ΔE, LASER8 adds M more nodes as a buffer to the grid. These nodes are laid down on a geometrically expanded buffer mesh where the expansion factor of each succeeding cell is given by 2^m, e.g., the first added cell has width $2\ \Delta X$, the second $4\ \Delta X$, etc. Thus the total width of this buffer is $\sum_{m=1}^{M} 2^m\ \Delta X$ into the slab. After the buffer is added, only the NMAX + M-th node is considered to be at ambient conditions, the enthalpy and temperature of all the other nodes are calculated using the finite-difference equations described in Sec. 3.4. Although an expansion rate of 2^m has worked well with all the problems to date, there may be times when another rate is desired. This rate is set in a module of the program, as discussed in Appendix A.

5.2 Phase Front Location and Velocity

Strictly speaking the position of a phase front in a finite-difference calculation cannot be determined with greater accuracy than one cell width. If the mushy zones discussed in Section 4.2 extend across more than one cell, the location and even the definition of phase fronts become uncertain. However, in those cases in which a mushy zone does not extend more than

one finite cell width it is possible to interpret the fraction of the latent heat of melting given up by the cell (i.e., the transition ratio of Sec. 4.2) as defining the position of the melt front within the cell. In a one-dimensional calculation the procedure is particularly simple because the position of the melt front can be determined straightforwardly from the melt fraction by linear interpolation. This is how LASER8 treats the problem of locating a single melt front. In those cases in which more than one melt front is present in the material at the same time, the present version of LASER8 follows only the front nearest the surface. However, after a calculation is over the movements of all fronts can be determined from the final output showing the history of all the cells (see, e.g. Figs. 6.8 and 6.9).

At each time step the state of every cell is specified. If a particular cell is known to be in a mushy state, its enthalpy will change from one time step to another while its temperature remains constant. The change in enthalpy can be interpreted as a change in the position of the melt front and this change divided by the fundamental time interval gives the velocity of the melt front. The difficulty with this procedure is that the time step is so small ($\sim 10^{-14}$ sec) that the position of the melt front may oscillate about the true position and give large fluctuations in magnitude and sign of the velocity. This can have serious implications for certain applications of LASER8 because some of the program switches may be based on the velocity of the melt-front, as for example in the case in which it is known that a-Si is formed from c-Si when the melt-front velocity exceeds ~15–20 m/sec in 100 directions. Also, in the application of a boundary condition such as that of Eq. 2.4, it is necessary to know the velocity in

order to determine the interfacial undercooling. Finally, one may wish to base some switching on the condition that the melt front has reached its maximum penetration. This condition is most easily determined by monitoring the change in sign of the velocity, but it will be reliable only if spurious fluctuations in the velocity can be removed by an averaging procedure.

In order to define the front velocity with sufficient accuracy, it is necessary to carry out some form of averaging of the melt-front position over time before calculating the velocity. To do this we have used an equation of the form

$$\bar{v} = (\bar{d}_2 - \bar{d}_1)/N\Delta t \ , \tag{5.1}$$

with

$$\bar{d}_2 = \sum_{i=1}^{n} d_2(t_i)/n; \ d_1 = \sum_{i=1}^{n} d_1(t_i)/n \ . \tag{5.2}$$

n is the number of consecutive time intervals over which the distances d_2 and d_1 are averaged to determine $\bar{d}_2$ and $\bar{d}_1$ to be used in Eq. 5.1. The choice of values of n and N to use in a given calculation should be related to the magnitude of $\bar{v}$ and how it changes with time. Presumably n can always be taken << N and in many cases it may be sufficient to take n = 1.

5.3 Treatment of Thermal Conductivity

Primarily because of the existence of mushy cells, the best method for dealing with the thermal conductivity in a finite-difference treatment of a moving boundary problem is not obvious. As a consequence, we carried out extensive testing of three different methods for treating the conductivity under the assumptions that the phase front is sharp and that its position

is given by the solid fraction of the cell, as discussed above. It can be seem from Eq. 3.10 that the effective conductivity between two cells has been taken as the average of the conductivity of the material in each of the two cells. This is the standard approach used in most finite-difference calculations, but problems can be expected when one or both of the cells contain slush. The problem is particularly troublesome when the conductivities of the material composing the slush differ greatly. Figure 5.1 shows the thermal conductivity of c-, a-, and ℓ-Si as a function of temperature; also shown is the specific heat. The value of K for a-Si is an order of magnitude less than that for ℓ-Si. The question then concerns the value of K to be assigned to a cell containing a changing mixture of phases as the melt front moves through.

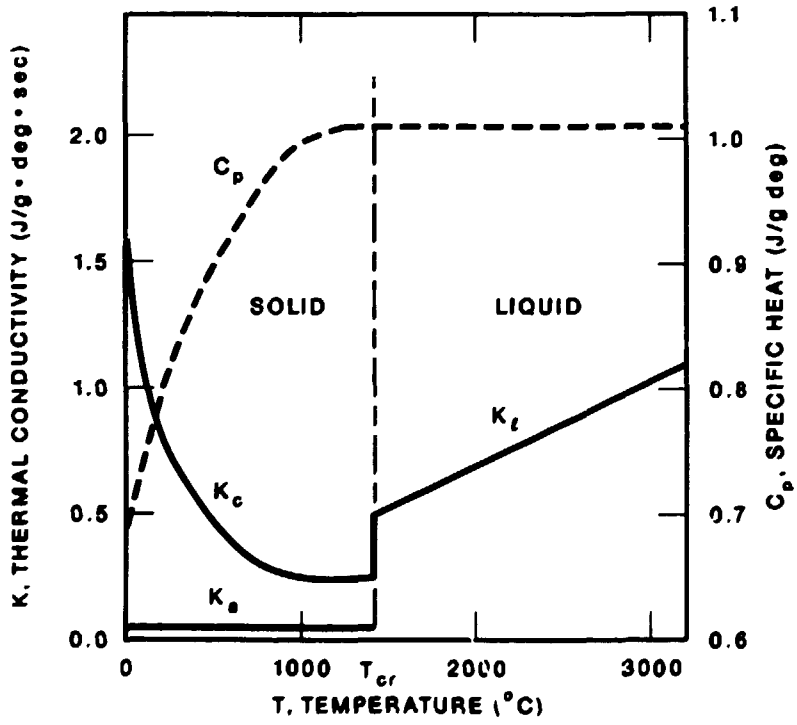

Fig. 5.1. Thermal conductivity (K) and specific heat (C_p) as a function of temperature for the various phases of silicon.

In the first method tried, an equivalent conductivity in a mushy cell was calculated from the equation

$$\frac{1}{K_e} = \frac{X_s}{K_s} + \frac{(1-X_s)}{K_\ell} \tag{5.3}$$

or

$$\frac{1}{K_e} = \frac{K_s K_\ell}{X_s K_\ell + (1-X_s)K_s} \tag{5.4}$$

Here, X_s is the solid fraction and K_s and K_ℓ are the thermal conductivities of the solid (crystalline or amorphous) and liquid, respectively. This conductivity was then used in Eq. 3.10 to determine the conductivity between cells. Intuitively this method is the most physically reasonable of the three tried. Unfortunately its implementation in the calculation led to nonphysical behavior of the temperature near the melt front. As a melt front moved through a cell, oscillations of the temperature in the neighboring cells were set up that worsened as the range over which the conductivities varied increased.

The second method was similar to the first except the effective conductivity of a cell was assumed to vary according to the relationship

$$K_e = X_s K_s + (1-X_s)K_\ell. \tag{5.5}$$

This method reduced the temperature oscillations seen with the first method but did not eliminate them. As the mesh was refined, the magnitude of the oscillations decreased, confirming that this behavior was nonphysical.

The third and final method tried was the simplest and gave the best results in the discrete formulation. In this method the conductivity was

assumed to be constant as a melt front moved across a cell. The conductivity between cells was taken to be the average of conductivities of adjacent cells. This method eliminated the oscillations, leaving only the step changes in temperature present in all three methods and caused by the change of phase process.

5.4 Analytical Approximations of Numerical Functions

Input data such as the thermal conductivity and specific heat as a function of temperature, the temporal shape of the laser pulse, and the various segments of the state diagram (T = T(e)) will generally be given as numerical functions. To make the computer program as efficient as possible, it was decided to approximate these functions by analytical forms so that table look-up and interpolation subroutines could be avoided.

All of the functions used in the program can be approximated by simple analytical forms over one or more ranges of the independent variable. Study of the program listing given in Appendix B will show that the excimer laser pulse shape used in some of the test calculations has been approximated by two quadratics, the function used to describe the temperature as a function of enthalpy was obtained by solving a quadratic for e(T), and the thermal conductivity of c-Si was approximated by an exponential, while that of ℓ-Si was approximated by a straight line.

Obviously, a user who prefers to work directly with numerical functions can easily modify the program to make this possible.

6.0 Results of Test Calculations

In this section results of several test problems will be considered. The accuracy of LASER8 was explored using two problems with analytic solutions as well as by comparison with results from HEATING5. Information on the performance and efficiency of the program was gathered while running several test cases which are described fully in Ref. 25. Finally, the results of a multiphase laser annealing example are given to demonstrate some of the unusual capabilities of LASER8. All the tests and examples were run on the IBM 3033's of Oak Ridge National Laboratory.

6.1 Accuracy Tests

The accuracy of the LASER8 program was tested by comparison of the finite-difference solutions with solutions of two problems that can be solved analytically. One of these problems does not involve a phase change and will be discussed in Sec. 6.2; it is given in Carslaw and Jaeger[21] as problem VI on page 80. The other problem, also given in Ref. 21 (page 287, problem III), involves the propogation of a melt front into a material and represents a fairly stringent test of LASER8; we discuss it first as a test of accuracy.

The problem considered first deals with a semi-infinite sample in which the solid is initially at a constant temperature T_{in} less than the melting temperature T_c. For all $t > 0$ the surface is held at some temperature $T_{sur} > T_c$. Expressions for the melt-front position and the temperature profiles in the liquid and solid as a function of time are given in analytical form. The test problem was simplified by assuming the thermal

properties of the liquid and solid to be the same. The temperatures T_{in}, T_c, and T_{sur} were taken to be 0°C, 50°C, and 100°C, respectively. The temperature profiles generated by the analytic solution and by LASER8 at a time 1.301 sec after t = 0 differed by less than 0.5 degrees except at the position of the melt front where the differences were somewhat higher, as might be expected. The maximum absolute error of the finite-difference calculations is large at early times because of the difficulty in treating the step change in temperature at the surface. However, this error quickly damps out and is less than a half a degree at 1.5 sec.

We concluded from the results of the tests calculations mentioned in this subsection that LASER8 gives an excellent approximation to the solutions of the analytical test cases.

6.2 Test Runs

a) Linear Picosecond Test Problem

The experiment simulated involves a constant-intensity laser pulse of 200 psec duration impinging on the surface of a silicon wafer assumed to have the constant optical and thermal properties given in Table 6.1.

Figure 6.1 shows the location of the melt front as a function of time. The two curves were generated by HEATING5 and LASER8, as indicated on the figure. Shortly after the laser pulse stops, at 200 psec, the liquid silicon begins to recrystallize and the melt front to retreat back to the surface. Both codes show complete resolidification at about 1.26 nsec. Figure 6.2 is an enlargement of the region around the onset of melting on Fig. 6.1.

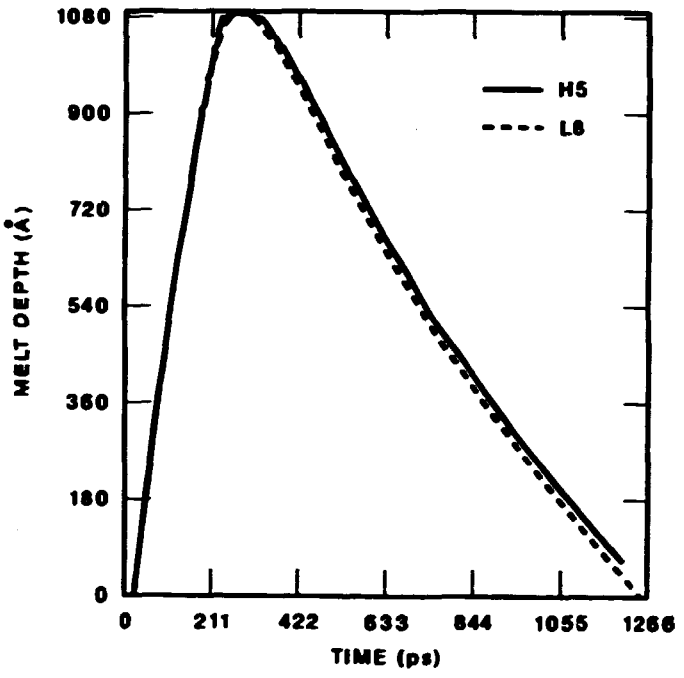

Fig. 6.1. A comparison of the melt front profiles generated by LASER8 (L8) and HEATING5 (H5) for the linear picosecond test case.

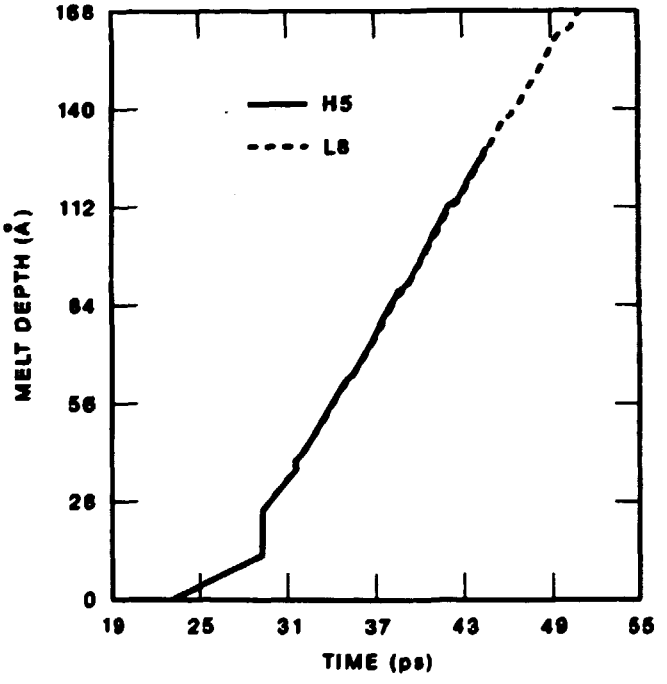

Fig. 6.2 The region around the onset of melting for the curves of Fig. 6.1.

Table 6.1. Input data for the linear picosecond test case.

Variable	Value	Units	Description
E_ℓ	0.3	J/cm^2	incident laser energy
t_ℓ	10^{-10}	sec	pulse half width
R	0.6	--	surface reflectivity
α	10^6	cm^{-1}	absorption coefficient
K	1.5	J/g deg sec	thermal conductivity
C_p	1.0	J/g deg	specific heat
ρ	2.33	g/cm^3	density
L	1500	J/g	latent heat
T_c	1410	°C	melting temperature
T_{in}	20	°C	initial temperature

The "scallops" evident in this figure are inherent in a finite volume formulation, with the size of the scallops dependent on the cell size used in the discretization. From Figs. 6.1 and 6.2 it is evident that the agreement between the two calculations is excellent even though some quite different numerical techniques are used in the two computer programs.

The temperature at the surface produced by the models is also of interest. The rapid increase in surface temperature produced by the laser pulse is shown in Figure 6.3. When the pulse is over, the surface temperature quickly drops to the melting temperature where it remains until solidification is complete; this is the same behavior generally found in this

type of calculation[4]. Figure 6.4 provides a detailed examination of the surface temperature at the onset of melting. As we would expect, the temperature remains constant at T_c for the short time it takes the first cell to melt. It then begins a stair-step rise as each successive cell accumulates the energy required for the melting process. As the distance between the melt front and the surface increases, the effect of the scalloping of the melt depth in Fig. 6.2 is reduced because of the increasing amount of liquid silicon. The rise in surface temperature on Fig. 6.4 becomes smoother the farther the melt front penetrates into the sample and away from the surface.

An analytic solution for this heat conduction problem is possible before the onset of melting. Temperature profiles at 8.25 psec after the beginning of the laser pulse are shown in Fig. 6.5; obviously there is again excellent agreement between the analytic and LASER8 solutions. This figure provides good evidence that the cell width used for these runs, $\Delta X = 25 \times 10^{-8}$ cm, was adequate to accurately resolve the laser energy profile.

b) Nonlinear Picosecond Test Problem

The constant properties used in the problem above are not realistic because both the thermal conductivity and the specific heat vary with temperature. From measured values of these properties, either table look up procedures or fitted analytic functions can be used to obtain the values at a given temperature.

The nonlinear picosecond case differed from the linear one in only two respects. First, the values for C_p and K were temperature dependent. The LASER8 code used a fitted function to evaluate the properties while the

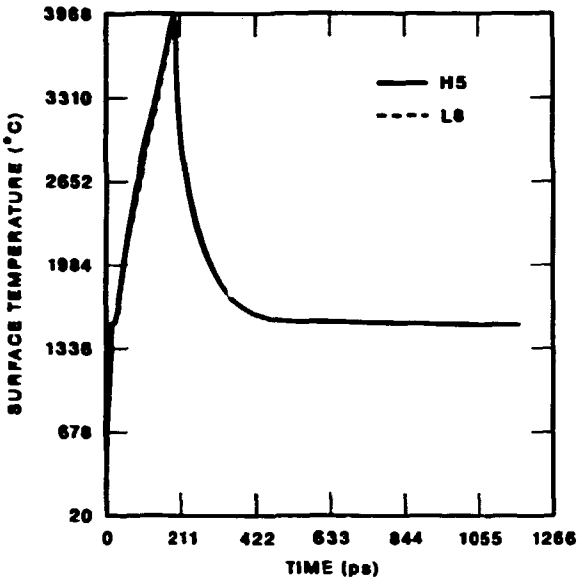

Fig. 6.3. Surface temperature as a function of time for the linear picosecond test case.

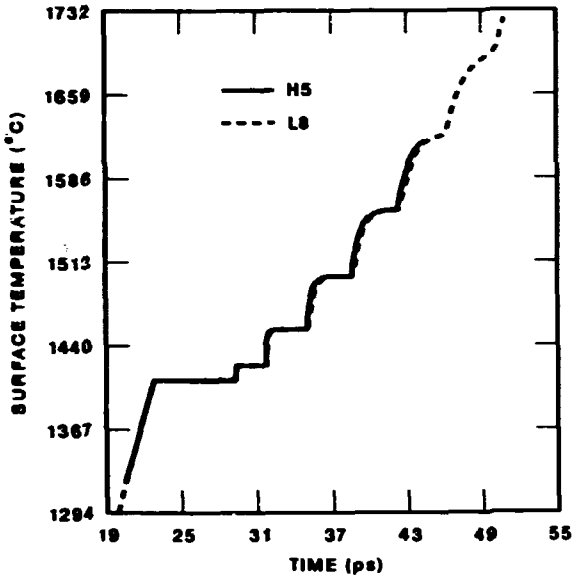

Fig. 6.4. The curve of Fig. 6.3 in the region near the onset of melting.

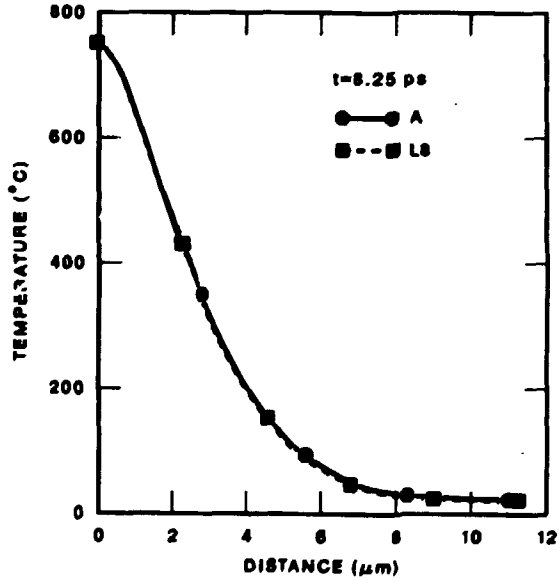

Fig. 6.5. Comparison of analytic (A) and LASER8 (L8) temperature profiles for the linear picosecond test case at a time before melting occurs. t is the time after the beginning of the laser pulse.

HEATING5 code used linear interpolation between tabular values. Second, the energy density was lowered to 0.1 J/cm^2 so that the surface would not vaporize before the pulse was over. Vaporization in the linear problem was not allowed although the temperature exceeded the vaporization point briefly. The thermal conductivity of silicon falls rapidly with temperature to a value much less than that shown in Table 6.1 (see Fig. 5.1). As a consequence a pulse of 0.3 J/cm^2 would cause excessive surface vaporization.

Figure 6.6 compares the computed melt depths and surface temperatures from HEATING5 and LASER8 calculations. Again excellent agreement between the results obtained with the two codes was found. The calculations with HEATING5 were terminated after ~300 psec because of the long running time on the computer.

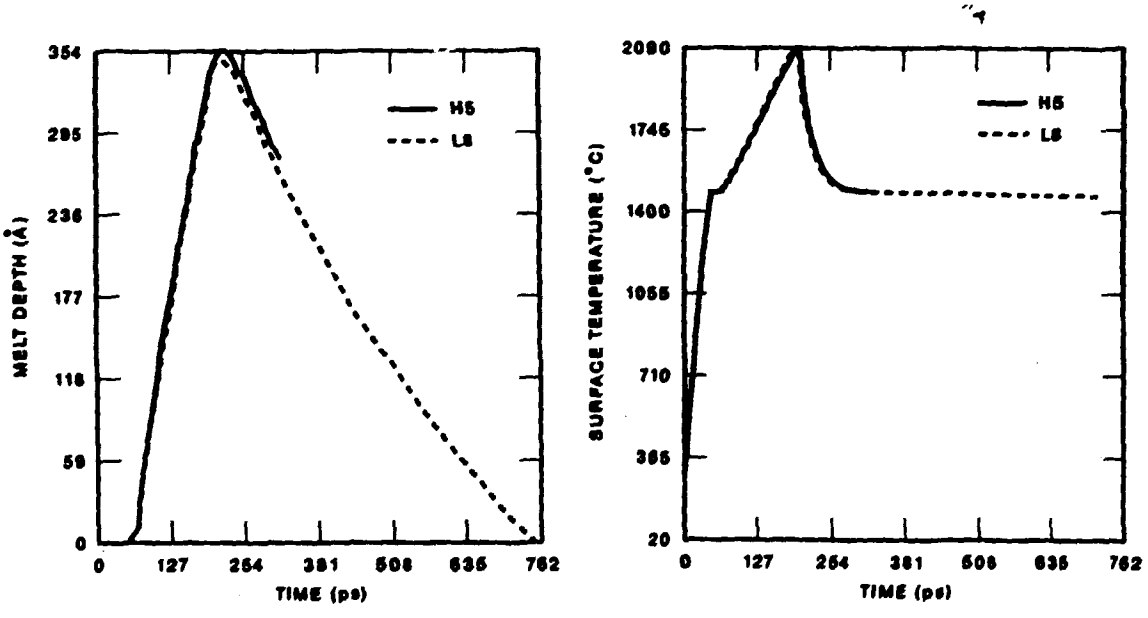

Fig. 6.6. Comparison of melt depth and surface temperature as a function of time from LASER8 (L8) and HEATING5 (H5) calculations for the for the nonlinear picosecond test case.

c) Nanosecond Test Problem

In additional testing of LASER8, we ran a problem with a triangular (isoceles) pulse of 20 nsec FWHM using temperature-dependent values of the thermal conductivity but a constant value of the specific heat (C_p = 1 J/g deg). These choices were made in order to reduce the differences introduced by the use of analytical (LASER8) and numerical (HEATING5) functions for C_p and the pulse shape. Figure 6.7 shows the comparison of the melt-front profiles obtained with the two programs at energy densities of 1.2 and 1.4 J/cm^2. The agreement is very good with the greatest differences being less than the finite-difference cell size of 100 Å. Correspondingly good agreement was also obtained for the surface temperature as a function of time, but we will not show that here.

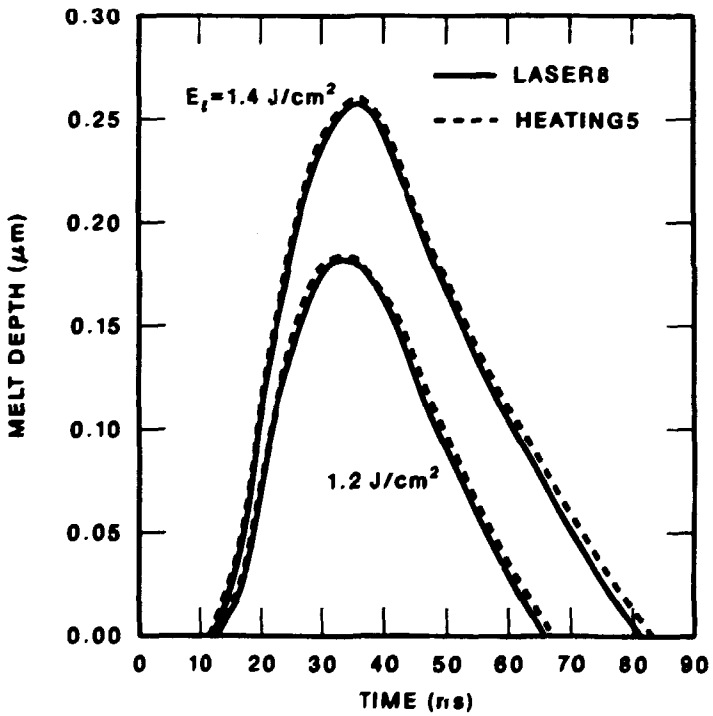

Fig. 6.7. Comparison of melt-front profiles obtained from LASER8 and HEATING5 calculations for energy densities of 1.2 and 1.4 J/cm^2.

6.3 Performance Comparisons

A study was made to compare the computational efficiencies, or performance, of LASER8 with HEATING5 and with two research codes developed during the evolution of LASER8. The results of these studies are discussed in Ref. 25 and will be summarized only briefly here. First, however, we again emphasize that LASER8 was designed to study problems inaccessible to HEATING5, and that as a consequence the programming philosophy of the two programs is quite different. To be more specific, the constraints imposed by the state array and by temperature-dependent thermal and optical properties made it difficult, and probably undesirable, to employ in LASER8 some of the numerical techniques used in HEATING5. For example, HEATING5 uses Levy's modification of the classical explicit procedure (see page 10 of Ref. 3) to speed up the calculations by adjusting the time step as the calculation proceeds. The introduction of the Levy technique into LASER8 was judged to be undesirable because of the requirement of energy conservation while iterating on the state array.

For problems in which the time step was held constant during a calculation, LASER8 was found to be more than a factor of ten faster than HEATING5. However, when HEATING5 was run with the Levy option to adjust the time step, the running times became comparable for calculations such as those leading to Fig. 6.7. Presumably, any type of accelerator introduced into LASER8 would result in it again being faster; this might be a direction for the future development of the program but because of the state array considerable care will be needed to ensure that stability conditions and conservation of energy are not violated.

6.4 A Complex Multiphase Laser Annealing Example

In order to demonstrate the unusual capabilities and flexibility of LASER8, a more complex example than those used in the test cases given above will now be considered. The basic problem corresponds exactly to that shown schematically in Fig. 2.1. One version of its state diagram is shown in Fig. 4.2 and discussed extensively in Section 4. We will not provide the details of the problem and the choice of input data here except to remark that the a-Si layer was 1900 A thick, the cell size was 100 A, and the laser pulse shape corresponded very closely to that shown in Fig. 3.2. Instead, attention is drawn to the richness of the results that can be obtained, as illustrated in the following discussion which considers how the effects of bulk nucleation and the phenomena of "explosive crystallization" can be simulated. We emphasize that the examples given here are not intented to closely replicate experimental results; they were chosen simply to illustrate the power of LASER8.

Figures 6.8 and 6.9 are reproductions of one form of the computer output, with lines indicating the boundaries between various regions drawn in by hand. The letters on a figure indicate the state of each finite-difference cell at the time printed on the left hand side. The letters have the following correspondence: C → c-Si; A → a-Si; S → ℓ-Si below T_c (supercooled); L → ℓ-Si at T_c or above; F → fine-grained polycrystalline material, and P → large-grained polycrystalline material.

a) Bulk Nucleation

Figures 6.8a-c show the type of behavior that follows from a simulation in which bulk nucleation, leading to the formation of fine-grained

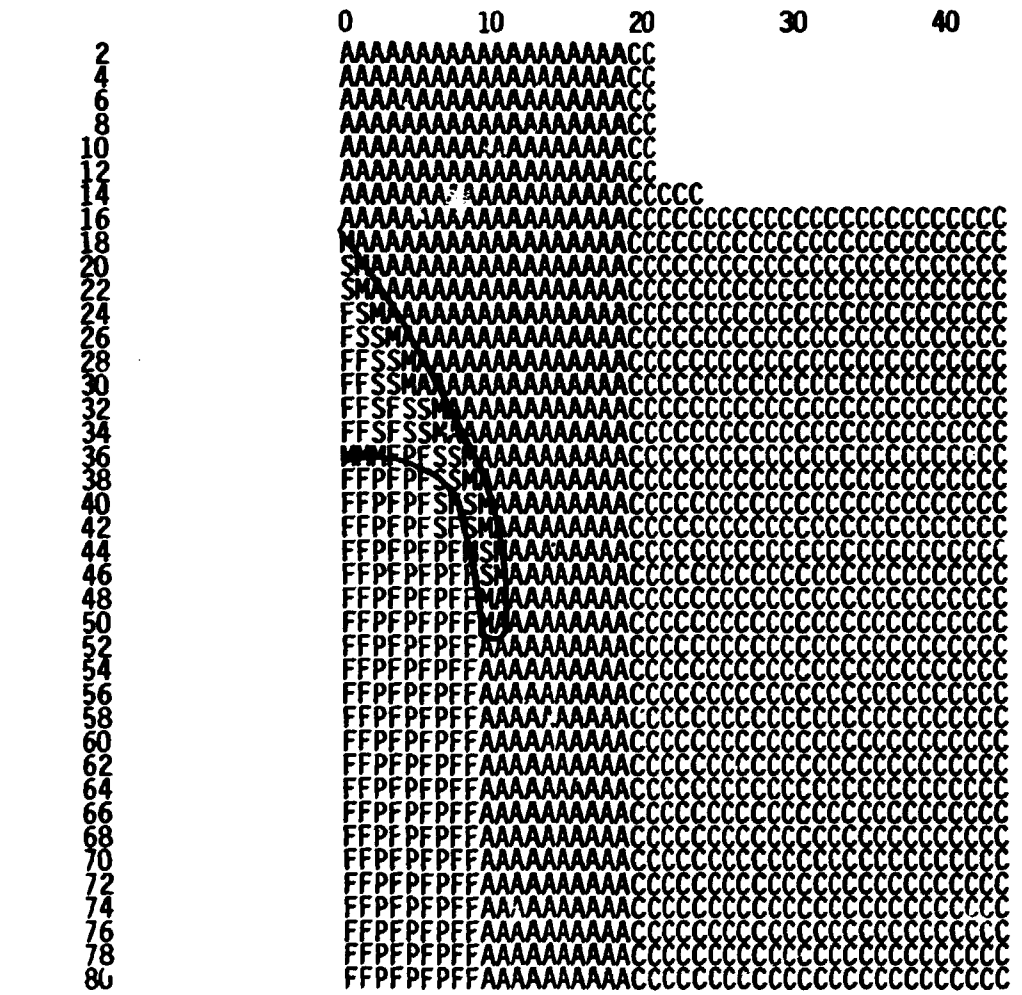

Fig. 6.8a. Melting and solidification of an a-Si layer on a c-Si substrate irradiated with an excimer laser pulse of 0.2 J/cm^2. The state array was set up to simulate bulk nucleation. Each letter except the left-most represents a cell size of 100 A; the surface cell is 50 A.

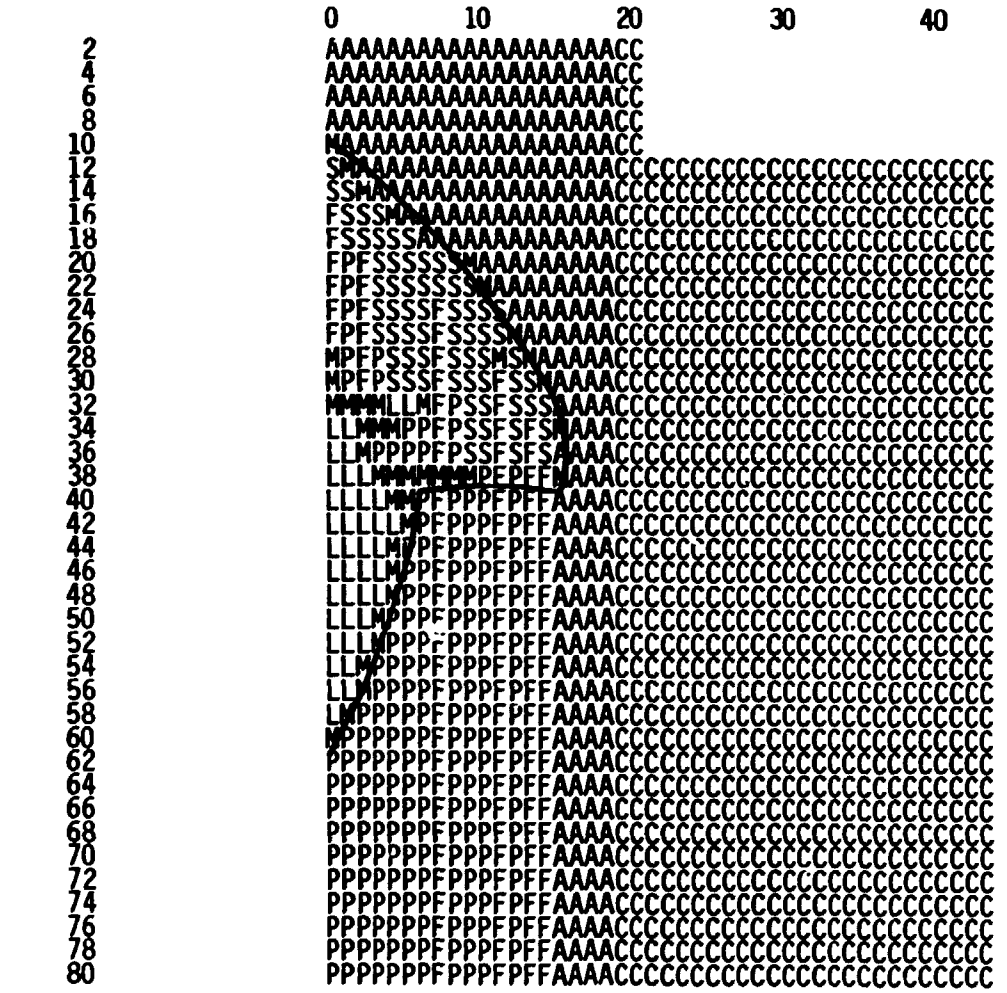

Fig. 6.8b. Same as Fig. 6.8a but for E_ℓ = 0.4 J/cm^2.

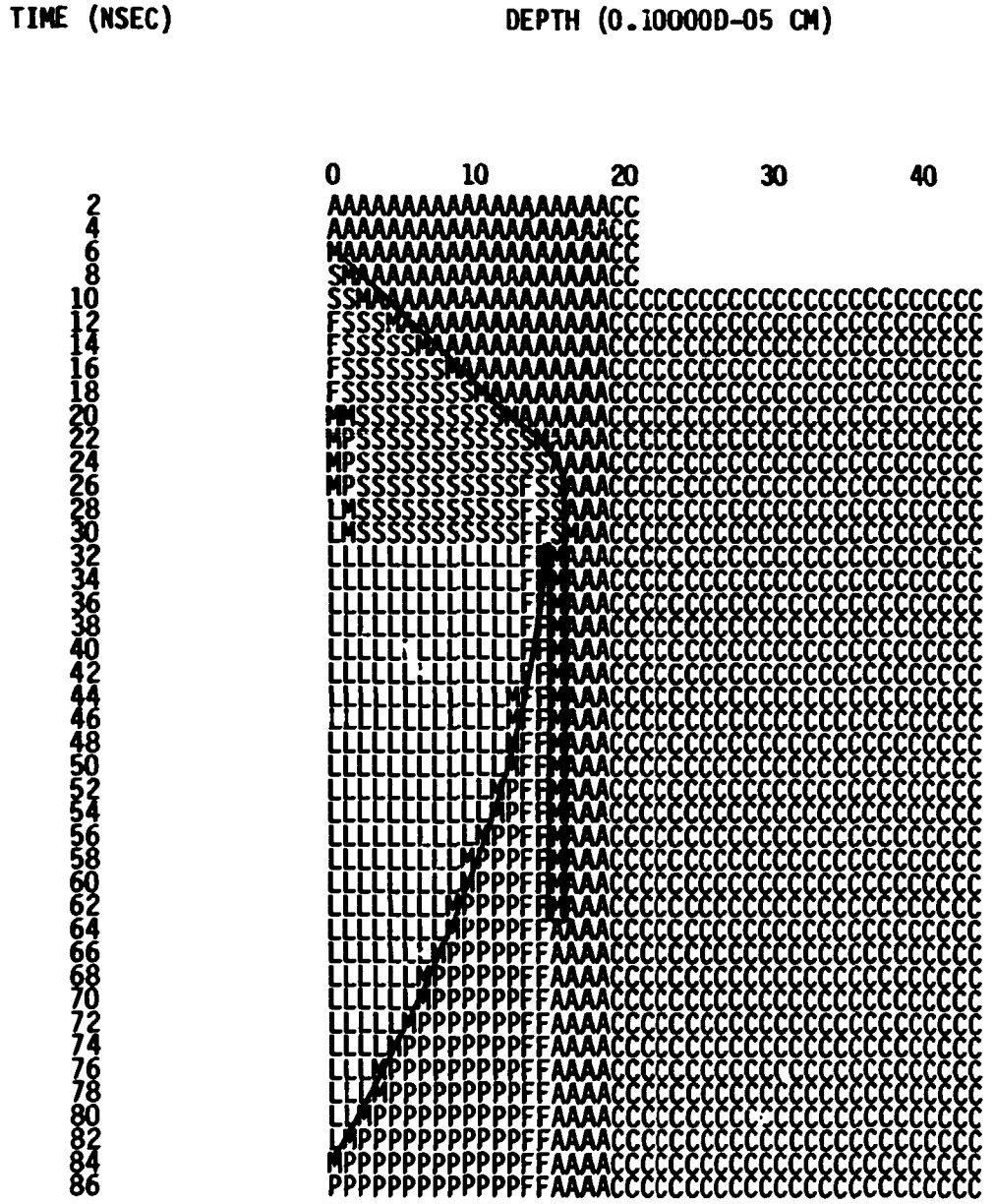

Fig. 6.8c. Same as Fig. 6.8a but for E_ℓ = 0.6 J/cm^2.

polycrystalline material, was forced to play a prominent role. From Fig. 6.9a, which shows the results of a calculation for E_ℓ = 0.2 J/cm^2, we see that the material in the first finite-difference cell began to melt at ~18 nsec and so became mushy (M). The nucleation timer was set at 4 nsec and consequently the first cell nucleated at 22 nsec, followed by nucleation of the second cell at 26 nsec; the nucleation temperature T_n, set at 1250° for these calculations, was never exceeded in these cells before the nucleation event. During the time from 22 to 38 nsec, the region from the surface to the melt front consisted of a mixture (slush) of solid and supercooled liquid due to bulk nucleation events. The penetration of the melt front into the a-Si was produced primarily by the release of latent heat. This effect becomes particularly apparant after 36 nsec when the surface region had solidified but a buried molten layer continued to penetrate into the solid, driven by the release of the latent heat of crystallization (L_c = 1800 J/g) which is greater than the latent heat of melting of a-Si (L_a = 1319 J/g). This effect is very similar to explosive crystallization described below but differs from it in that the latent heat is released by successive nucleation events rather than by growth from a solid-liquid interface trailing behind the melt front (see Fig. 6.9a). The resolidified layer is shown as being composed of a mixture of FG and LG p-Si, but experimentally the LG material with 200 A grain size would be indistinguishable from the FG material with 100 A grain size.

Next, we consider the sequence of events illustrated on Fig. 6.8b for a laser pulse energy of 0.4 J/cm^2. At ~10 nsec the first cell began to melt and 4 nsec later nucleation occurred in it; by the time the first cell nucleated the melt front had penetrated to the fifth cell (~500 A). By the

30th nsec, additional nucleation events and the formation of FG material have occurred in the 3rd, 8th, and 11th, resulting in an extended region filled with a mixture of phases and states. At the 38th nsec the maximum melt front penetration has been reached, most of the mixed region has solidified, while the temperature of the molten material near the surface has risen above 1410°C, as indicated by an L in the surface cells. Finally, at ~60 nsec, the melt front originating from this near-surface region returns to the surface and solidification is complete. The appearance of a LG p-Si region within approximately 10 cells of the surface and a FG region in the 11th to 15th cells in the solidified material was dictated by conditions specified in the state array, which were chosen to qualitatively simulate the experimental observations.

Figure 6.8c shows the results for E_ℓ = 0.6 J/cm^2. Nucleation occurs only at the surface and near the liquid-solid interface. This behavior results from the fact that although for times less than 30 nsec the majority of the liquid is undercooled for longer than 4 nsec, bulk nucleation does not occur in most cells because the temperature is above the nucleation temperature. Only when the melt front pauses at its deepest penetration is the liquid below T_n for the 4 nsec required for nucleation. For times greater than 32 nsec, the temperatures of all molten cells, including that of the remelted surface cell, are above the melting point of c-Si at T_c = 1410°C. The melt front subsequently returns to the surface in a manner typical of c-Si at a velocity of ~4 m/sec.

b) Explosive Crystallization

Figures 6.9a-c show the results of calculations designed to simulate a somewhat different physical phenomena than that of Figs. 6.8a-c. Whereas

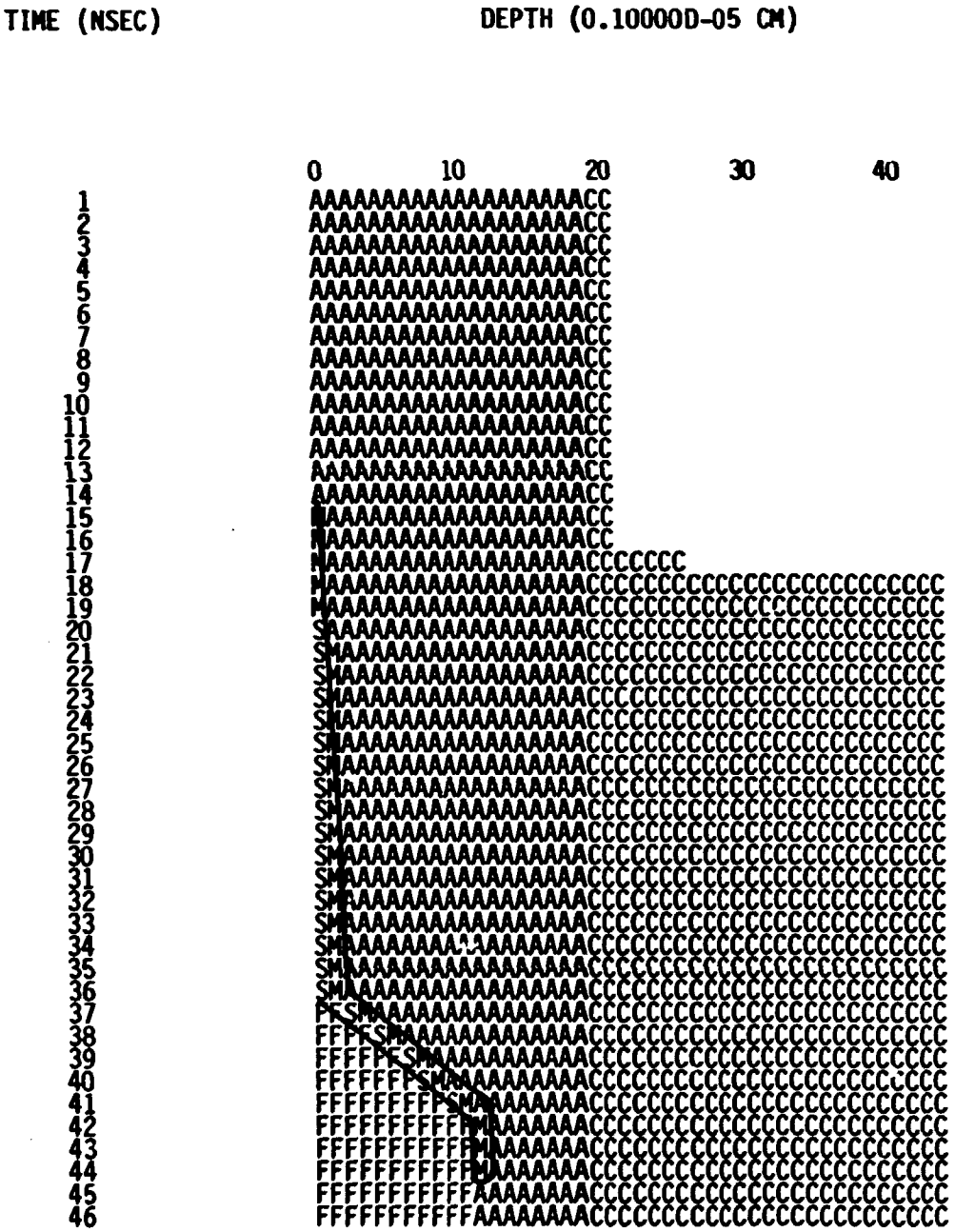

Fig. 6.9a. Results of a calculation similar to that of Fig. 6.8a but with the LASER8 program modified to simulate "explosive crystallization". The energy density was 0.15 J/cm^2.

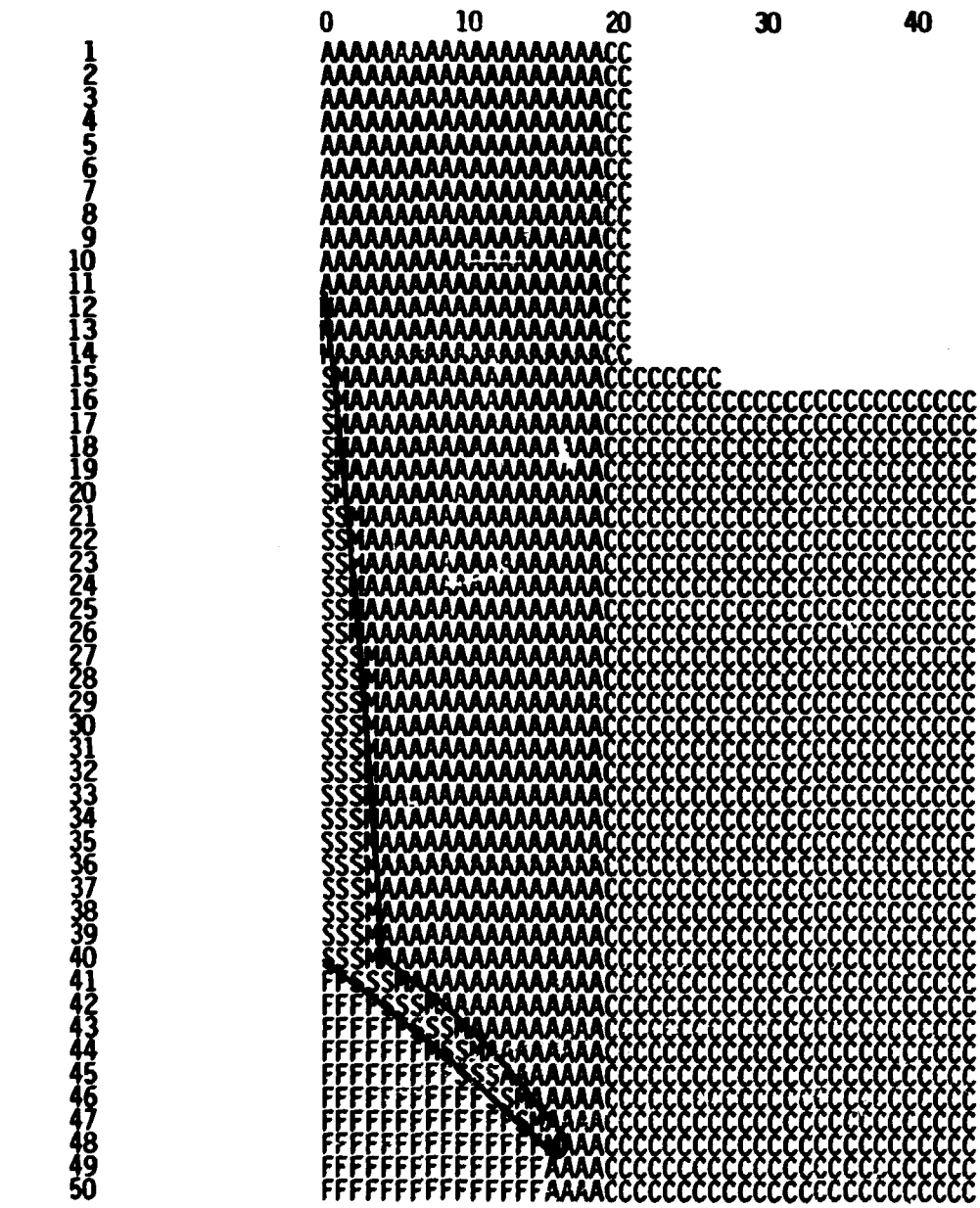

Fig. 6.9b. The same as Fig. 6.9a but with E_ℓ = 0.2 J/cm^2.

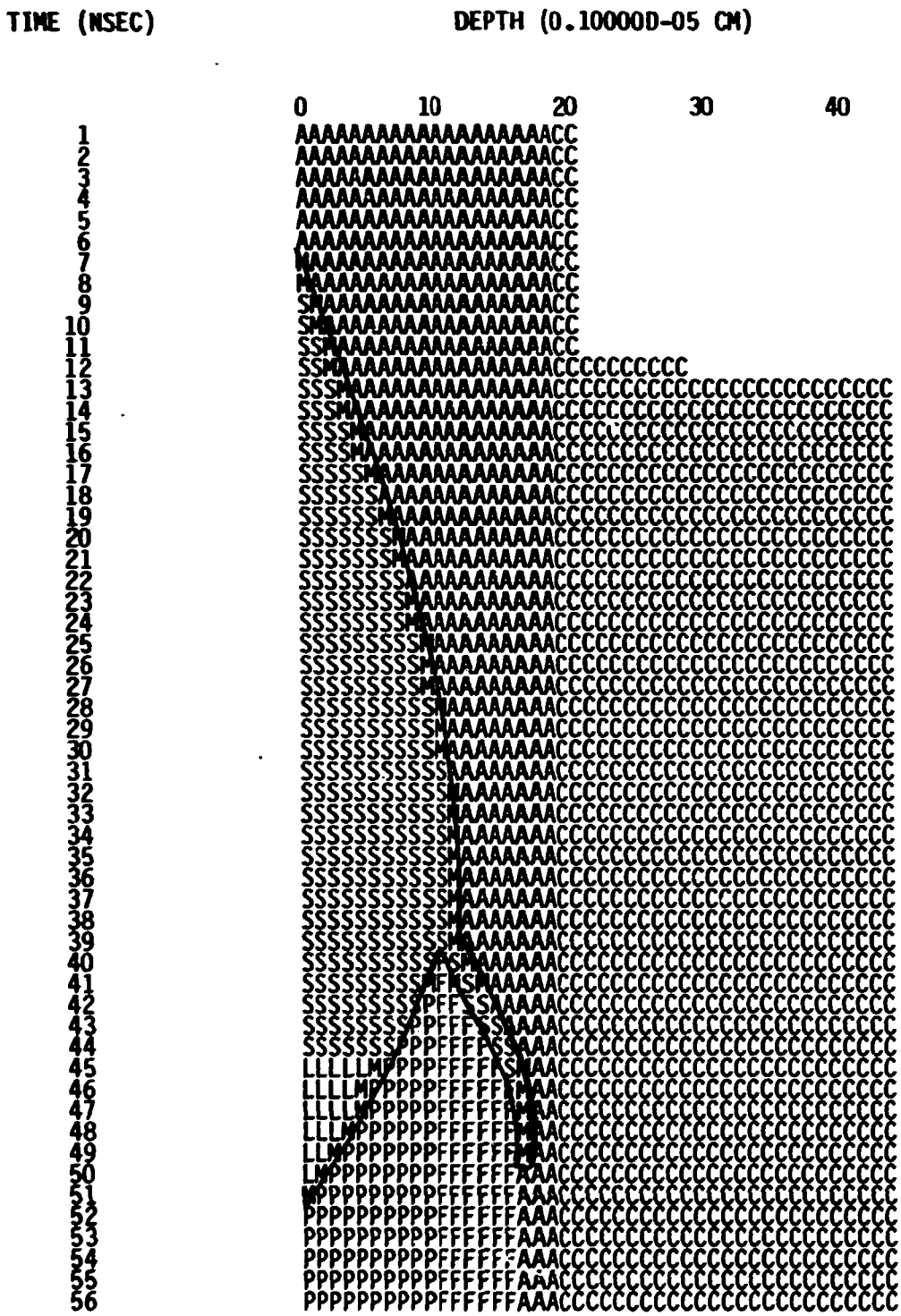

Fig. 6.9c. The same as Fig. 6.9a but with E_ℓ = 0.4 J/cm^2.

the modeling leading to the latter allowed bulk nucleation to occur throughout an extended region, the calculations discussed here confined the nucleation events (indicated by the first appearance of FG material) to a region very near or at the interface. Once a nucleation event occurred, the newly solidified material was allowed to serve as a seed for further growth thus making additional nucleation events unnecessary.

Figure 6.9a shows what might be described as a pure explosive crystallization process. The laser pulse with E_ℓ = 0.15 J/cm^2 caused the surface to melt at 15 nsec and the melt front initially just barely penetrated beyond the first cell. The basic LASER8 program was modified slightly to require that the nucleation of polycrystalline silicon be suppressed until after the melt front just began to return to the surface (by monitoring the sign of the melt-front velocity). The release of latent heat then drove the melt front into the next cell in a manner similar to that shown in Fig. 6.8a. However, in the present case, polycrystalline material was allowed to grow off the already crystallized layer at the surface so that after each new cell was melted it could resolidify by using the cell adjacent to it on the surface side as a seed.

Figures 6.9b and c show the evolution of the solidification behavior as the energy density is first increased to 0.2 J/cm^2 and then to 0.4 J/cm^2. This behavior can be described as a mixture of normal and explosive crystallization, with Fig. 6.9c showing the simultaneous propagation of a buried molten layer into the solid and a more normal return of the melt front to the surface from the initially nucleated cell.

7.0 Concluding Remarks

In this report we have described the conceptual basis, the development, and the usage of the computer program LASER8. Here we wish to emphasize again that LASER8 is primarily a research tool, designed to have the capability of investigating some of the most difficult problems presented by the experimental results on pulsed laser processing of semiconductors, such as Si, Ge, and GaAs. These problems are associated primarily with ultrarapid melting and solidification and include the role of undercooling and overheating in a phase change, the way in which interfacial kinetics influence the undercooling, and the way in which phase nucleation can be simulated in a heat flow calculation. Because definitive solutions to these problems are not yet known, our treatment of them will continue to be studied intensively, with the result that LASER8 will undergo continual evolution. It is really not appropriate then to speak of a single computer code called LASER8 that can be used routinely as a tool to study engineering type problems. We believe the ideas and numerical techniques underlying LASER8 are much more important than the code itself. Consequently, those who choose to use LASER8 are encouraged to experiment freely with it if they feel so inclined.

The illustrative examples given in the report are just that, and not intended to reflect our current thinking on the problems they represent. For example, the very complex solidification behavior and morphologies of a pulsed laser irradiated a-Si overlayer on a c-Si substrate are still being studied intensively and the results shown on Figs. 6.8 and 6.9 are meant only to illustrate that complexity. The results of more refined studies of this problem will be reported in later publications.

Another comment in this same vein concerns the other problem discussed in Sec. 2 which stimulated the development of LASER8, i.e., the transformation of c-Si to a-Si by pulsed laser irradiation. The picosecond test cases of Figs. 6.1 and 6.6 show regrowth velocities of ~100 m/sec, well above the velocity at which a-Si should be formed although we did not allow for it. The processes involved in this transformation almost certainly involve very strong undercooling of the liquid during the return of the melt front to the surface. Although LASER8 provides a framework for including this undercooling, the exact way in which it is to be incorporated into a calculation has not been discussed here. This too is a research problem we hope to report on shortly.

Finally, it should be apparant that the techniques used in LASER8 are applicable to a much wider class of problems than those of laser annealing of semiconductors. Obviously the same techniques can be applied to rapid heating and cooling of metals, insulators, and ceramics. Silicon has been emphasized in this report because it was the material entering most prominently in the development of laser annealing. As we have seen, a-Si has a latent heat associated with its melting and solidification that is almost as great as that of c-Si (Fig. 4.1). True glassy materials do not melt or solidify in this way. LASER8 should provide a powerful tool for the study of the glass transformation in glass forming materials because of the great flexibility provided by the state diagram and the state array.

Acknowledgements

We would like to thank V. Alexiades, J. B. Drake, G. E. Giles, G. E. Jellison, Jr., D. H. Lowndes, and A. D. Solomon for many useful discussions bearing on topics covered in this report.

References

1. Several general references on this subject are "Pulsed Laser Processing of Semiconductors," ed. by R. F. Wood, C. W. White, and R. T. Young in the Semiconductor and Semimetals Series ed. by R. K. Willardson and A. C. Beer, Academic Press, New York (1984); "Laser Annealing of Semiconductors," ed. by J. M. Poate and J. W. Mayer, Academic Press (1982); and the volumes in the series of Proceedings of the Materials Research Society, published by North-Holland.
2. HEATING5 is a recent version of a computer program HEATING which was originally developed by several groups of workers. HEATING is an acronym for Heat Engineering and Transfer in Nine Geometrics. HEATING5 is described at length in Ref. 3.
3. HEATING5 - An IBM 360 Heat Conduction Program, W. D. Turner, D. C. Elrod, and I. I. Siman-Tov, ORNL/CSD/TM-15 (1977). Available from National Technical Information Service, U.S. Department of Commerce.
4. R. F. Wood and G. E. Giles, Phys. Rev. B 23, 2923. This paper describes some of the modifications made to HEATING5 to adapt it to calculations of the effects of pulsed laser irradiation of semiconductors. See also Chapter 4 of Ref. 1.
5. Semiconductor processing with cw lasers is also of general interest, but since melting seldom occurs in applications of cw lasers we restrict our attention to pulsed lasers.
6. R. Tsu, R. T. Hodgson, T. Y. Tan, and J. E. Baglin, Phys. Rev. Lett. 42, 1356 (1979).
7. P. L. Liu, R. Yen, N. Bloembergen, and R. T. Hodgson, Appl. Phys. Lett. 34, 864 (1979).

8. A. G. Cullis, H. C. Weber, N. G. Chew, J. M. Poate, and P. Baeri, Phys. Rev. Lett. 49, 219 (1982).

9. E. P. Donovan, F. Spaepen, D. Turnbull, J. M. Poate, and D. C. Jacobson, Appl. Phys. Lett. 42, 698 (1983).

10. A. G. Cullis, Mat. Res. Soc. Symp. Proc. 13, 75 (1983).

11. H. C. Webber, A. G. Cullis, and N. G. Chew, Appl. Phys. Lett. 43, 669 (1983).

12. D. H. Lowndes, R. F. Wood, and J. Narayan, Phys. Rev. Lett. 52, 561 (1984).

13. M. O. Thompson, G. J. Galvin, J. W. Mayer, P. S. Peercy, J. M. Poate, D. C. Jacobson, A. G. Cullis, and N. G. Chew, Phys. Rev. Lett. 52, 2360 (1984).

14. J. Narayan and C. W. White, Appl. Phys. Lett. 44, 35 (1984).

15. R. F. Wood, D. H. Lowndes, and J. Narayan, Appl. Phys. Lett. 44, 770 (1984).

16. Indications of such features are found in Ref. 14, and they play a prominent role in recent data of D. H. Lowndes and coworkers (to be published).

17. K. A. Jackson and B. Chalmers, Can. J. Phys. 34, 473 (1956).

18. D. Turnbull, Solid State Phys. 3, 225 (1956).

19. See Chapter 5 of Reference 1 and references therein.

20. See Chapter 4 of Reference 1 and references therein.

21. See, for example, H. S. Carslaw and J. C. Jaeger "Conduction of Heat in Solids," Second Edition, Clarendon Press, Oxford (1959) p. 282.

22. J. R. Cannon in "Moving Boundary Problems," edited by D. G. Wilson, A. D. Solomon, and P. T. Boggs, Academic Press, New York (1978), p. 3.

23. J. H. Holloman and D. Turnbull, Progr. Metal Phys. IV, 333 (1953).

24. C. S. Hsu and A. Rahman, J. Chem. Phys. 70, 5234 (1979).

25. V. Alexiades, J. B. Drake, G. A. Geist, G. E. Giles, A. D. Solomon, and R. F. Wood, "Mathematical Modeling of Laser-Induced Ultrarapid Melting and Solidification," Oak Ridge National Laboratory Report No. ORNL-6129.

26. We feel it would be unproductive to go into detail here about the relative merits of finite-difference and finite-element techniques.

27. M. Rose, Math. Comput. 14, 249 (1960).

28. A. Solomon, Math. Comput. 20, 347 (1966).

29. See M. von Allmen, Mat. Res. Soc. Symp. Proc. 13, 691 (1983) for the application of an enthalpy equation to a laser quenching problem.

30. This condition is unlikely to hold at a rapidly moving interface between two phases of greatly different densities.

31. A good example is contained in the article "A Mushy Zone Model With an Exact Solution" by A. D. Solomon, D. G. Wilson, and V. Alexiades, Letters in Heat and Mass Transfer 9 , 319 (1982).

Appendix A

A Guide to the Use of LASER8

A.0 Introduction

LASER8 is controlled through four input lists: DIMEN, PULSE, BCIC, and MATPRP. These set values of parameters associated with the finite-difference calculation, the laser pulse, the initial conditions, and the material properties respectively. In the version of LASER8 described here, starting conditions are limited to a pure crystal, an amorphous layer on a crystalline substrate, an all amorphous material, or restarting from any configuration of the nine allowable states shown in the state array of Fig. 4.4. The laser pulse can have any user-defined profile (a specific excimer laser profile is given in the program listing in Appendix B) or the user may wish to use the triangular or square pulse approximations built into the code. A triangular pulse is often a satisfactory approximation to a gaussian or a skewed gaussian.

LASER8 is written in modular, top-down programming. Thus modifications can be made inside a module, for example by adding other states or materials into the module "UPDATE NODE STATES", or entire modules can be removed and replaced with compatible modules. Of course, a series of similar problems can be run just by modifying the input parameters. A description of all the input quantities follows.

INPUT LIST	MEMBER		DESCRIPTION
DIMEN			
	N	=	number of nodes actually being calculated; it should initially be large enough to fully describe the penetration of the laser radiation into the material.

NMAX = maximum number of nodes that will be used (< 240); once NMAX is reached 10 nodes are extended into the slab to a depth of 1024 times DX.

DX = constant space step used for entire problem.

NVS = number of time steps between two averaged melt-front positions used in a velocity calculation.

NVW = number of time steps used in averaging the melt-front position for use in a velocity calculation.

DTOUTG = time step between state graph outputs.

DTOUTD = time step between temperature and energy profile outputs.

PULSE

TH = half the total width of the pulse.

EL = energy density of the pulse.

ALPHA = absorption coefficient of material at the wavelength of the laser pulse.

RS,RL = reflectivity of solid and liquid, respectively.

ISHAPE = 1 for a square pulse,
2 for a triangular pulse, and
3 for a user supplied pulse profile (area must be normalized to unity).

BCIC

TINIT = initial temperature of entire slab.

XA = depth of the amorphous layer; XA = 0 if no amorphous layer is present.

ISTART = 0 if starting time = 0.0, and
1 if a restart file continuing from a set of conditions is to be read.

MATPRP

TD = decision value for TIMER1

TP = decision value for TIMER2; usually taken as the time required for a critical nucleus to form in a cell in a supercooled melt.

RHO = density of material; presently assumed constant and equal for all phases.

TA = melt temperature of amorphous material.

HA = latent heat of amorphous material.

TN = temperature above which a critical nucleus cannot form in a supercooled melt.

HC = latent heat of crystalline material; polycrystalline material assumed to have same value.

TC = melt temperature of crystalline and polycrystalline material.

CL = specific heat of liquid material (assumed constant).

A.1 Inputing a Laser Pulse Profile

To input a laser pulse profile into LASER8 the module labeled CALCULATE ABSORBED LASER ENERGY PROFILE must be modified. Certain properties of the profile are assumed by the code and care must be taken that these are met. First, for any given profile, the area should be determined and used to normalize the area under the new profile to unity. The normalized numerical profile should then be piecewise fit with some continuous functions, e.g., parabolas. Usually two or three parabolas are sufficient. For continuous profiles the area is normalized by dividing the functional representation by the original area.

Inside the module labeled CALCULATE ABSORBED LASER PROFILE are three sections. The first is for a square pulse. The second is for a triangular (isosceles) pulse. The third is for a user supplied normalized profile. The first line of this section must be labeled with 89 and the last line of the section is GO TO 86. The profile is inserted in the following form:

S1 = S1*PULDUR*(value of profile at this time).

If the profile is a piecewise fit of several curves and/or straight lines, then this line would be preceded by an IF test like:

IF(TIME.LE.end of piece one) S1 = S1*PULDUR*(...),

and so on for each of the pieces of the profile. The profile is a function of TIME which is the elapsed time in seconds since the pulse began. The other variables, S1 and PULDUR, are described in the following section.

A.2 Variables used in LASER8

Here we give an alphabetical listing of all the variables used in LASER8 and a short description of each.

ALPHA	Absorption coefficient of the material at the laser wavelength
CL	Specific heat of liquid material
DE	Difference in enthalpy between crystal and amorphous phases at the melt temperature of amorphous material
DELTAE	Increase in enthalpy needed before a new node is added
DEPTH	Depth of the melt front
DIFMAX	Maximum diffusivity of the material - used to determine stability criterion
DT	Time step
DTOUTD	Time between outputs of temperature and energy profiles
DTOUTG	Time step between state graph outputs
DX	Constant space step used for entire problem
E()	Enthalpy array
EA	Enthalpy at which amorphous material begins to melt
EAINIT	Initial enthalpy in amorphous cells

EC	Enthalpy at which crystalline material begins to melt
ECINIT	Initial enthalpy in crystalline cells
EIN	Enthalpy above which no nucleation occurs
EL	Energy density of the pulse
ELA	Enthalpy above which amorphous material is liquid
ELC	Enthalpy above which crystalline material is liquid
HA	Latent heat of amorphous material
HC	Latent heat of crystalline material
IPHASE	State number of a particular cell (see ISTATE)
ISHAPE	Selects type of laser pulse profile
ISTART	Selects restart from stored data or no restart
ISTATE()	Array of the state of each cell
K()	Array of the conductivities of each cell
KAKL	Average of K-amorphous and K-liquid
KCKL	Average of K-crystal and K-liquid
KEQL	Equivalent conductivity across left boundary of cell
KEQR	Equivalent conductivity across right boundary of cell
KFKL	Average of K-fine grain and K-liquid
N	Number of nodes being calculated
NMAX	Maximum number of nodes that dynamic rezone allows
NSTATE()	Output array of state of each cell as a single letter
NVS, NVW	Number of time steps used in calculating melt-front velocity
PULDUR	Total pulse duration
RATIO	Stability criterion for explicit method $< 1/2$
RHO	Density of material
RL	Reflectivity of liquid in the surface region

RS	Reflectivity of solid in the surface region
S()	Array of the fraction of surface energy absorbed in a cell
S1	Laser energy at the surface
SCONST	Constant used to calculate S1
T()	Temperature array
TA	Melt temperature of amorphous material
TC	Melt temperature of crystalline material
TD	Decision value for TIMER1
TH	Half the total pulse duration
TIME	Time from the beginning of the pulse
TIMER1()	Array of timers for comparison to TD
TIMER2()	Array of timers for comparison to TP
TINIT	Initial temperature of the material
TN	Temperature above which nucleation cannot occur
TOUTD	Time step between temperature and enthalpy profile outputs
TOUTG	Time step between state graph outputs
TP	Decision value for TIMER2
W	Constant used in updating enthalpy

A.3 How LASER8 Works: Description of Principal Modules

Whenever a module must delineate between the many possible states the material of a finite-difference cell might be in, a computed GOTO statement is used. In the version of LASER8 given in Appendix B and discussed here, each label in the GOTO statements is a two digit number. The first digits correspond to the ISTATE numbers and have the following correspondence:

1=crystalline	2=LG polycrystalline	3=FG polycrystalline
4=amorphous	5=mushy4	6=mushy1
7=mushy3	8=liquid	9=supercooled

The second digit is constant for a given computed GOTO statement, for example, it is 0 in the module labeled UPDATE NODE STATES. These labels are kept in numerical order. For efficiency, state calculations are combined when they are identical. For example, the conductivity of liquid and supercooled liquid are assumed to be the same function of temperature so there would be only one label for both in the GOTO statement for the calculation of thermal conductivity. If labels are necessary between the computed GOTO cases, they have three digits and their leading digit is the ISTATE number. An example of this can be seen in the UPDATE NODE STATES module of the listing in Appendix B.

If it is desired to add different materials or simply more states to the STATE ARRAY, new ISTATE numbers (10, 11, 12,...) can be added to the possible cases of each computed GOTO statement. Care should be taken that identical labels are not used in the program. If a conflict occurs, the above labeling criteria should take precedence over any other labeling scheme used in the program.

If a user wants only to modify a particular aspect of an existing state, he would go to the module that deals with that aspect and state and modify the appropriate lines; the labels will not be changed in this case.

READ IN INPUT PARAMETERS

This module reads in the four input lists: dimensional parameters, pulse parameters, initial conditions, and material properties. It then prints a header for the output.

CALCULATE MISC VALUES

With the input values established, this module initializes the time variables and calculates the largest stable time step. It also calculates various constants used in the program.

SWITCH CRITICAL TEMPERATURES INTO ENTHALPIES

This module takes the materials properties and the initial temperature and calculates the critical enthalpies on the temperature/enthalpy state diagram.

INITIALIZE ARRAYS WITH IC AND BC

This module uses TINIT, XA, and the enthalpies calculated in the preceding module to initialize the temperature, enthalpy, state, and S(heat generation) arrays.

LOAD RESTART VECTORS

If ISTART equals 1 then this module reads in restart data from unit 1 which will overwrite some and perhaps all of the initial conditions.

CALCULATE INITIAL CONDUCTIVITIES

Given the startup temperature array, this module calculates the initial conductivities K(T). The present module assumes the material is silicon. It uses a computed GOTO statement.

CALCULATE PERCENT OF ENERGY ABSORBED IN EACH CELL

This module uses DX and ALPHA to integrate EXP(-ALPHA*X) over each cell. It stores this value in the S array.

OUTPUT PARAMETER VALUES

Input parameter values are printed here, with the exception of the initial conditions which 'LOAD RESTART...' may have changed.

OUTPUT INITIAL VALUES

The temperature and enthalpy profiles are output at the initial time. This gives the initial condition of the slab even if 'LOAD RESTART...' is executed.

BEGIN TIME LOOP

Label for the beginning of the time loop. The value of NM1 is also set at this point.

FIND SURFACE REFLECTIVITY

Given ISTATE(), E(1), RS and RL, the surface reflectivity RO is calculated. The reflectivity changes linearly from RS to RL as the surface cell melts. This module uses a computed GOTO statement.

CALCULATE ABSORBED LASER ENERGY

Given the value of ISHAPE, this module selects the appropriate pulse profile and then calculates the amount of laser energy S1 transmitted through the surface during any time step. (Also see 'Inputing a Laser Pulse Profile'.)

UPDATE ENERGY BY ROSE'S SCHEME

This module updates the enthalpy array E(), by a scheme proposed by Rose. (See Sec. 3.)

CHECK DIFFUSION INTO MODEL

This module checks to see if thermal diffusion has raised the enthalpy in the deepest node above the limit set by DELTAE. If it has, then a new node is added to the grid, as described in Sec. 5.

CHECK IF NMAX IS REACHED

If N equals NMAX then a new node will not be added. Instead, E(NMAX) is found by extending 12 nodes deep into the slab. Each node is twice as wide as the previous one so the maximum depth reached by these nodes is greater than 4096 * DX. The accuracy will be degraded if NMAX is so low that the melt front reaches into this region.

UPDATE NODE STATES

This module uses a computed GOTO statement to update the timers, and the previous states of the cells from their values at the preceding time step.

DETERMINE CONDUCTIVITIES AND TEMPERATURES

The updated states and energies are used to calculate the new temperatures and conductivities for all the cells by a computed GOTO statement. The module shown here assumes the material is silicon.

FIND DEPTH AND VELOCITY OF FRONT CLOSEST TO SURFACE

Calculates melt-front penetration and velocity for the melt-front closest to the surface.

OUTPUT STATES

Output the NSTATE() array for each DTOUTG time step on unit 2. This produces a line printer graph of the state of each cell as a function of time. This module uses a computed GOTO statement.

OUTPUT TEMPERATURE AND ENTHALPY PROFILES

Output the T() and E() arrays for each DTOUTD time step on the standard unit.

CHECK IF TIME TO STOP

This module checks to see if it is time to stop the calculation. The criteria is as follows: First, do not stop while the pulse is still on. This makes the code robust in the sense that pulses that peak late or even double pulses can be modeled. Secondly, do not stop until the entire slab is solid. This criterion became necessary when mushy or liquid regions remained deep in the material after the pulse was off.

APPENDIX B

Program Listing

```
C
C                              *** LASER8 ***
C   LASER MELTING PROGRAM
C   ASSUMES TEMPERATURE DEPENDENT OPTICAL AND THERMAL PROPERTIES
C   ALLOWS FOR LAYERS OF AMORPHOUS,CRYSTALLINE,AND POLYCRYSTALLINE
C   INITIALIZE WHOLE ARRAY. CALCULATE ONLY CHANGING VALUES
C   LET N FOLLOW PROBLEM
C
C   FOR MORE INFORMATION CONTACT  AL GEIST
C                                 P.O. BOX Y Bldg. 9207A
C                                 OAK RIDGE NATIONAL LABORATORY
C                                 OAK RIDGE TN  37830
C
CCCCCCCCCCCCCCCCCCCCCCCCCCCCCCCCCCCCCCCCCCCCCCCCCCCCCCCCCCCCCCCCCCCCCCC
C
C  DESCRIPTION OF INPUT VARIABLES
C
C       N      = NUMBER OF NODES ACTUALLY BEING CALCULATED
C                SHOULD INITIALLY BE LARGE ENOUGH TO ENCOMPASS
C                LASER PENETRATION INTO MATERIAL
C
C       NMAX   = MAXIMUM NUMBER OF NODES THAT WILL BE USED < 240
C                ONCE NMAX IS REACHED 12 NODES ARE EXTENDED INTO
C                THE SLAB TO A DEPTH OF 4096 * DX
C
C       DX     = CONSTANT SPACE STEP USED FOR ENTIRE PROBLEM
C
C       NVS    = NUMBER OF TIME STEPS BETWEEN TWO AVERAGED MELT-FRONT
C                POSITION USED IN A VELOCITY CALCULATION.
C
C       NVW    = NUMBER OF TIME STEPS USED IN AVERAGING THE MELT-FRONT
C                POSITION FOR USE IN A VELOCITY CALCULATION.
C
C       DTOUTG= TIME STEP BETWEEN STATE GRAPH OUTPUTS
C
C       DTOUTD= TIME STEP BETWEEN TEMPERATURE AND ENERGY PROFILE OUTPUTS
C
C       TH     = HALF THE TOTAL WIDTH OF THE PULSE
C
C       EL     = ENERGY DENSITY OF THE PULSE
C
C       ALPHA  = ABSORPTIVITY OF MATERIAL AT THIS WAVELENGTH
C
C       RS, RL= REFLECTIVITY OF SOLID AND LIQUID RESPECTIVELY
C
C       ISHAPE= 1  SQUARE PULSE
C               2  TRIANGULAR PULSE
C               3  USER SUPPLIED PULSE PROFILE - AREA MUST EQUAL 1
C
C       TINIT  = INITIAL TEMPERATURE
C
C       XA     = DEPTH OF AMORPHOUS LAYER. 0 IF NONE
C
```

```
C      ISTART= 0  START AT TIME =0.0
C              1  READ RESTART FILE CONTINUE FROM THESE CONDITIONS
C
C      TP     = TIME REQUIRED FOR SURVIVABLE NUCLEUS TO EXIST IN
C               A REGION OF DX IN A SUPERCOOLED MELT.
C
C      TD     = NUCLEATION DELAY FOR FORMATION OF LARGE GRAIN POLY
C               OFF OF FINE GRAIN POLY IN A SUPERCOOLED MELT.
C
C      RH0    = DENSITY OF MATERIAL ASSUMED CONSTANT OVER PHASES
C
C      TA     = MELT TEMPERATURE OF AMORPHOUS MATERIAL
C
C      HA     = LATENT HEAT OF AMORPHOUS MATERIAL
C
C      TN     = TEMPERATURE ABOVE WHICH A SURVIVABLE NUCLEUS CANNOT
C               EXIST IN A SUPERCOOLED MELT
C
C      HC     = LATENT HEAT OF CRYSTAL AND POLYCRYSTALLINE MATERIAL
C
C      TC     = MELT TEMPERATURE OF CRYSTAL AND POLYCRYSTALLINE MATERIAL
C
C      CL     = SPECIFIC HEAT OF LIQUID MATERIAL ASSUMED CONSTANT.
C
C      VMAX   = MELT-FRONT VELOCITY AT WHICH AMORPHOUS MATERIAL FORMS
C
CCCCCCCCCCCCCCCCCCCCCCCCCCCCCCCCCCCCCCCCCCCCCCCCCCCCCCCCCCCCCCCCCCCCCCCCCC
C
      IMPLICIT REAL*8 (A-H,O-Z,K)
      CHARACTER*1 NSTATE(250)
      DIMENSION K(250),E(250),T(250),S(250),
     &          ISTATE(250),TIMER1(250),TIMER2(250)
C
      DATA TIMER1/250*0.0D0/,TIMER2/250*0.0D0/
C
C-----------------------------------------------------------------------
C  OPEN FILES FOR OUTPUT DATA
      OPEN(1,FILE='restart.dat')
      OPEN(2,FILE='state.dat')
      OPEN(6,FILE='temp.dat')
C
C-----------------------------------------------------------------------
C  READ IN DIMENSIONAL PARAMETERS
      READ *,N,NMAX,DX,NVS,NVW,DTOUTG,DTOUTD
C
C  READ IN LASER PULSE PARAMETERS
      READ *,TH,EL,ALPHA,RS,RL,ISHAPE
C
C  READ IN INITIAL AND BOUNDARY CONDITIONS
      READ *,TINIT,XA,ISTART
C
C  READ IN PHYSICAL PROPERTIES OF THE MATERIAL
      READ *,TP,TD,RH0,TA,HA,TN
```

```
      READ * ,HC,TC,CL,VMAX
C-----------------------------------------------------------------------
C  OUTPUT HEADING
      PRINT 100
  100 FORMAT(' ',23X,'LASER8',/' ',15('*'),' LASER ANNEALING ',
     &       'MODEL ',15('*')//)
C -----------------------------------------------------------------------
C  MISC VALUES
      TIME=0.0D0
      TOUTG=0.D0
      TOUTD=0.D0
      DEPTH=0.D0
      DEP1 =0.D0
      DEP2 =0.D0
      V    =0.D0
      VPROD=0.D0
      VAPRE=0.D0
      NCOUNT=0
      ICOUNT=0
      IFRMAX=0
      SUMS1=0.0D0
      PULDUR=2.0D0*TH
      KAKL=(0.02D0+0.4D0)*.5D0
      KCKL=(0.216D0+0.5D0)*.5D0
      KFKL=(0.1D-1+6.5D0)*.5D0
      K(NMAX)=1.6D0
C  DIFMAX = LARGEST DIFFUSIVITY ENCOUNTERED IN PROBLEM
C  FOR SILICON IT IS AT 20 DEGREES C
      DIFMAX=1.0D0
      RATIO=1.0D0/2.0D0
      DT=RATIO*DX*DX/DIFMAX
      W=0.5D0/(DX*DX*RH0)
      SCONST=EL/(2.0D0*RH0*TH*DX)
      RATDX2=RATIO*DX*DX*RH0
C -----------------------------------------------------------------------
C  SWITCH CRITICAL TEMPERATURES INTO ENTHALPIES
      EC=0.0D0
      ELC=HC
      ELA=CL*(TA-TC)+HC
      EA=ELA-HA
      DE=EA-(0.914259D0-DSQRT(0.8358693D0+.4676D-3*(TC-TA)))/.2338D-3
      EIN=(TN-TC)*CL+HC
      ECINIT=(.914259D0-DSQRT(.8358693D0+.4676D-3*(TC-TINIT)))/.2338D-3
      EAINIT=ECINIT+DE
C -----------------------------------------------------------------------
C  INITIALIZE ARRAYS WITH IC AND BC
      IX=0
      IF(XA.EQ.0.0D0) GO TO 6
      IX=XA/DX+.5D0
      DO 6 I=1,IX
      T(I)=TINIT
      E(I)=EAINIT
      S(I)=0.0D0
```

```
      ISTATE(I)=4
    6 CONTINUE
      IX=IX+1
      NMAXP=NMAX+13
      DO 6000 I=IX,NMAXP
      T(I)=TINIT
      E(I)=ECINIT
      S(I)=0.0D0
      ISTATE(I)=1
 6000 CONTINUE
C ------------------------------------------------------------------
C  FIND INITIAL ENERGY IN CELLS AT TIME 0 (ET0)
      IF(IX.EQ.0) THEN
        ET0=(NMAX-1)*ECINIT
      ELSE
        ET0=(IX-.5)*EAINIT+(NMAX-IX-.5)*ECINIT
      ENDIF
      DO 6010 I=1,12
      ET0=ET0+(ECINIT)*(2**(I-2)+2**(I-1))
 6010 CONTINUE
C ------------------------------------------------------------------
C  LOAD RESTART VECTORS
      IF(ISTART.EQ.0) GO TO 900
      READ(1,2100) TIME,N,DX,DT
      READ(1,2200) (T(M2),E(M2),ISTATE(M2),M2=1,N)
  900 CONTINUE
C ------------------------------------------------------------------
C  CALCULATE INITIAL CONDUCTIVITIES (K)
      DO 9 I=1,NMAXP
      IPHASE=ISTATE(I)
      GO TO (14,14,14,44,54,64,74,84,84),IPHASE
   14 K(I)=DEXP(-.399671D-2*T(I)+.365786D0)+.225894D0
      GO TO 9
   44 K(I)=0.02D0
      GO TO 9
   54 K(I)=KAKL
      GO TO 9
   64 K(I)=KCKL
      GO TO 9
   74 K(I)=KFKL
      GO TO 9
   84 K(I)=3.2435111D-4*T(I)+3.8711424D-2
    9 CONTINUE
C ------------------------------------------------------------------
C  STORE INITIAL STATE OF CELL 1 FOR CALCULATION OF MELT DEPTH
      IF(ISTATE(1).EQ.4 ) THEN
        EX1=EA
        ELX1=ELA
        HX1=HA
      ELSE
        EX1=EC
        ELX1=ELC
        HX1=HC
```

```
      ENDIF
C -------------------------------------------------------------------
C  CALCULATE PERCENT OF ENERGY ABSORBED IN EACH CELL
C  ASSUMING IT IS GENERATED IN THE SURFACE LAYERS
C  BY INTEGRATING [ALPHA EXP(-ALPHA*X)] OVER EACH CELL
      DPTH1=0.D0
      DO 7 I=1,N
      DPTH2=DX*(I-.5D0)
      IF(DPTH2.GE.5.D-5) GO TO 7000
      S(I)=DEXP(-ALPHA*DPTH1)-DEXP(-ALPHA*DPTH2)
      DPTH1=DPTH2
   7  CONTINUE
 7000 CONTINUE
C -------------------------------------------------------------------
C  OUTPUT INPUT VALUES
      PRINT 110
      PRINT 120 ,N,NMAX,DX,DTOUTG,DTOUTD,TH,EL,ALPHA,RS,RL,
     &          ISHAPE,TP,TD,RH0,TA,HA,TN,HC,TC,CL,VMAX
  110 FORMAT('    NAME          ALL UNITS KG W J CM SEC'/)
  120 FORMAT('    DIMEN',/'   N=',I3,' NMAX=',I3,' DX=',D10.4,
     &       ' DTOUTG=',D10.4,' DTOUTD=',D10.4,//
     &       '     PULSE',/
     &       '  HALF WIDTH (TH)=',D10.4,' LASER ENERGY (EL)=',D10.4,/
     &       '  ALPHA=',D10.4,' REFLECTIVITY(RS)=',F5.3,
     &       ' REFLECTIVITY(RL)=',F5.3,' ISHAPE=',I2,//'    MATPRP',/
     &       '  NUCLEATION TIME (TP)=',D10.4,
     &       ' NUCLEATION DELAY (TD)=',D10.4,/'  DENSITY (RH0)=',F5.3,/
     &       '  TCR AMORPHOUS (TA)=',F6.1,' LATENT HEAT (HA)=',F6.1,/
     &       '  NUCLEATION TEMP (TN)=',F6.1,' LATENT HEAT (HC)=',F6.1,
     &     /'  TCR CRYSTAL (TC)=',F6.1,' SPECIFIC HEAT (L)=',F6.3,
     &       ' VMAX =',F6.1)
C -------------------------------------------------------------------
C  OUTPUT INITIAL VALUES
      PRINT 150 ,TIME,DT
      PRINT 205
      PRINT 210 , (T(M2),M2=1,NMAX)
      PRINT 215
      PRINT 170 ,(E(M2),M2=1,NMAX)
  150 FORMAT(' ',//'  TIME =',D13.5,' SEC    DT='D13.5)
  170 FORMAT(' ',(12X,10(D10.4,1X)))
C -------------------------------------------------------------------
C  OUTPUT HEADING FOR LINE PRINTER GRAPH OF STATE VS  TIME
      WRITE(2,220)
      WRITE(2,230) DX
 230  FORMAT(' ',/'     TIME (SEC)',15X,'DEPTH (',D11.5,' CM)'//,17X,
     &       '0',8X,'10',8X,'20',8X,'30',8X,'40',8X,'50',8X,'60',8X,
     &       '70')
C
C ===================================================================
C
C  BEGIN TIME LOOP
  27  NM1=N-1
      IF(N.GT.NMAX) NM1=NMAX-1
```

```
C ------------------------------------------------------------
C  FIND SURFACE REFLECTIVITY (R0)
      IPHASE=ISTATE(1)
      GO TO (12,12,12,12,52,62,62,92,92),IPHASE
  12  R0=RS
      GO TO 1000
  52  SF=(ELA-E(1))/HA
      R0=RS*SF+RL*(1.0D0-SF)
      GO TO 1000
  62  SF=(ELC-E(1))/HC
      R0=RS*SF+RL*(1.0D0-SF)
      GO TO 1000
  92  R0=RL
C ------------------------------------------------------------
C  CALCULATE ABSORBED LASER ENERGY PROFILE
 1000 IF (TIME.GT.PULDUR) GO TO 840
C  DEFAULT IS SQUARE PULSE
      S1=SCONST*DT*(1.0D0-R0)
      GO TO (86,87,89),ISHAPE
C  TRIANGULAR PULSE
  87  IF(TIME.LE.TH) S1=2.0D0*TIME*S1/TH
      IF(TIME.GT.TH) S1=2.0D0*(S1-(TIME-TH)*S1/TH)
      GO TO 86
C  USER SUPPLIED NORMALIZED PROFILE (AREA UNDER CURVE = 1)
C  THIS IS AN EXCIMER PROFILE
 89   IF(TIME.LT.40.D-9) GO TO 841
        S1=S1*PULDUR*(7.84728D7+TIME*(-2.33377D15+1.74295D22
     &                                          *TIME))
      GO TO 86
 841  IF(TIME.LT.16.D-9) GO TO 842
        S1=S1*PULDUR*(2.74602D7+TIME*(4.03853D14-1.91274D22
     &                                          *TIME))
      GO TO 86
 842  S1=S1*PULDUR*(2.46685D6+TIME*(3.45003D15-1.11884D23
     &                                          *TIME))
      GO TO 86
C
 840  S1=0.0D0
  86  CONTINUE
      SUMS1=SUMS1+S1
C ------------------------------------------------------------
C  UPDATE ENERGY (E) BY ROSE'S SCHEME
      E(1)=E(1)+2.0D0*(W*DT*(K(1)+K(2))*(T(2)-T(1))+S1*S(1))
      DO 2 I=2,NM1
      KEQL=(K(I-1)+K(I))
      KEQR=(K(I)+K(I+1))
      E(I)=E(I)+W*DT*(KEQR*(T(I+1)-T(I))
     &              +KEQL*(T(I-1)-T(I))) +S(I)*S1
   2  CONTINUE
C
C  CHECK FOR SIGNIFICANT DIFFUSION INTO MATERIAL
C  ADD RIGHTMOST NODE AS NECESSARY
      IF(N.LT.IX) GO TO 580
```

```
      DELTAE=ECINIT+.25D0
      GO TO 581
  580 DELTAE=EAINIT+.25D0
  581 CONTINUE
      IF(E(NM1).LT.DELTAE) GO TO 1400
      IF(N.GE.NMAX) GO TO 57
C   ADD NODE
      N=N+1
      GO TO 1400
C   IF NMAX REACHED FIND E(NMAX) BY EXTENDING 12 NODES DEEP INTO THE SLAB
C   EACH NODE IS TWICE AS WIDE AS THE PREVIOUS ONE
C   THE EXPANSION RATE IS ADJUSTED WITH THE 2**I TERMS
   57 N=NMAXP
      E(NMAX)=E(NMAX)+W*DT*((K(NMAX+1)+K(NMAX))*(T(NMAX+1)-T(NMAX))
     &                     +(K(NMAX)+K(NMAX-1))*(T(NMAX-1)-T(NMAX)))
      DO 1400 I=1,12
      NI=NMAX+I
      KEQL=3.D0*K(NI-1)*K(NI)/(K(NI)+2.D0*K(NI-1))
      KEQR=3.D0*K(NI)*K(NI+1)/(K(NI+1)+2.D0*K(NI))
      E(NI)=E(NI)+2.D0*W*DT/(2**I+2**(I-1))*(KEQR*(T(NI+1)-T(NI))/(2**I)
     &                                      +KEQL*(T(NI-1)-T(NI))/(2**(I-1)))
 1400 CONTINUE
C ------------------------------------------------------------------------
C
C   UPDATE NODE STATES :     1=CRYSTAL    2=LARGE POLY 3=FINE POLY
C                            4=AMORPHOUS  5=MUSHY4     6=MUSHY1
C                            7=MUSHY3     8=LIQUID     9=SUPERCOOLED
      DO 1100 I=1,NM1
      IF(I.EQ.1) THEN
        IM1=2
      ELSE
        IM1=I-1
      ENDIF
      IPHASE=ISTATE(I)
      GO TO (10,10,30,40,50,60,70,80,90),IPHASE
   10 IF(E(I).GE.EC) ISTATE(I)=6
      GO TO 1100
   30 IF(E(I).GE.EC) ISTATE(I)=7
      GO TO 1100
   40 IF(E(I).GE.EA) ISTATE(I)=5
      GO TO 1100
   50 IF(E(I).LT.EA) ISTATE(I)=4
      IF(E(I).GE.ELA ) ISTATE(I)=9
      GO TO 1100
   60 IF(E(I).GT.ELC) GO TO 601
      IF(E(I).LT.EC)  GO TO 602
      IF(V .GE. -VMAX) GO TO 1100
      IF(E(I).GT.EA) ISTATE(I)=5
      IF(E(I).GT.ELA) ISTATE(I)=9
      GO TO 1100
  601 ISTATE(I)=8
      GO TO 1100
  602 IF(ISTATE(I+1).EQ.1 .OR. ISTATE(IM1).EQ.1) GO TO 603
```

```
      ISTATE(I)=2
      GO TO 1100
  603 ISTATE(I)=1
      GO TO 1100
   70 IF(E(I).LT.EC) ISTATE(I)=3
      IF(E(I).GT.ELC) ISTATE(I)=8
      GO TO 1100
   80 IF(E(I).LT.ELC) GO TO 801
      GO TO 1100
  801 IF(ISTATE(I+1).LT.4 .OR. ISTATE(IM1).LT.4) GO TO 802
      ISTATE(I)=9
      GO TO 1100
  802 ISTATE(I)=6
      GO TO 1100
   90 IF(E(I).GE.ELC) GO TO 906
      IF(E(I).LT.ELA) GO TO 905
      IF(E(I).LT.EIN) GO TO 901
      TIMER2(I)=0.D0
      GO TO 902
  901 TIMER2(I)=TIMER2(I)+DT
  902 IF(ISTATE(I+1).EQ.1) GO TO 907
      IF(ISTATE(I+1).LT.4 .OR. ISTATE(IM1).LT.4) GO TO 903
      TIMER1(I)=0.D0
      GO TO 904
  903 TIMER1(I)=TIMER1(I)+DT
  904 IF(TIMER1(I).GT.TD) ISTATE(I)=6
      IF(ISTATE(I).EQ.6 .AND. ISTATE(I-1).EQ.3) ISTATE(I)=7
      IF(TIMER2(I).GT.TP) ISTATE(I)=7
      GO TO 1100
  905 ISTATE(I)=5
      GO TO 1100
  906 ISTATE(I)=8
      GO TO 1100
  907 ISTATE(I)=6
 1100 CONTINUE
C ---------------------------------------------------------------------
C
C  DETERMINE CONDUCTIVITIES (K)  ••• HARDWIRED FOR SILICON •••
C  DETERMINE TEMPERATURES (T)
      DO 1 I=1,N
      IPHASE=ISTATE(I)
      GO TO (11,11,31,41,51,61,71,81,81),IPHASE
   11 T(I)=1410+E(I)*(.9142589998D0-1.169196D-4*E(I))
      K(I)=DEXP(-.00399671D0*T(I)+.365786D0)+.225894D0
      GO TO 1
   31 T(I)=1410+E(I)*(.9142589998D0-1.169196D-4*E(I))
      K(I)=.10D0
      GO TO 1
   41 EI=E(I)-DE
      T(I)=1410+EI*(.9142589998D0-1.169196D-4*EI)
      K(I)=0.015D0
      GO TO 1
   51 T(I)=TC+(E(I)-HC)/CL
```

```
      IF(T(I).GT.3267.D0) T(I)=3267.D0
      K(I)=3.2485111D-4*T(I)+3.8711424D-2
      GO TO 1
   51 T(I)=TA
      K(I)=KAKL
      GO TO 1
   61 T(I)=TC
      K(I)=KCKL
      GO TO 1
   71 T(I)=TC
      K(I)=KFKL
    1 CONTINUE
C ------------------------------------------------------------------
C
C  FIND DEPTH OF FRONT CLOSEST TO THE SURFACE
      IF(E(1).LT.EX1) GO TO 894
      DPTHM1=DEPTH
      IF(E(1).GT.ELX1) GO TO 891
      DEPTH=0.5D0*DX*E(1)/HX1
      GO TO 894
  891 DO 892 I=2,N
      IF(ISTATE(I).GT.4 .AND. ISTATE(I).LT.8) GO TO 893
      IF(ISTATE(I).LT.5) GO TO 897
  892 CONTINUE
      GO TO 894
C
C  NEXT THREE STATEMENTS ARE FOR MELT FRONT AT CELL BOUNDARY
  897 IFRNT=I
      DEPTH=DX*(IFRNT-1.5D0)
      GO TO 894
  893 IFRNT=I
      HX=HC
      IF(ISTATE(I).EQ.4) HX=HA
      DEPTH=DX*(I-1.5D0)+DX*E(I)/HX
  894 CONTINUE
C
C  CALCULATE VELOCITY OF THE FRONT CLOSEST TO SURFACE
      VAPRE=V
      NCOUNT=NCOUNT+1
      IF(NCOUNT.LE.(NVS-NVW/2)) GO TO 895
      DEP2=DEP2+DEPTH
      IF(NCOUNT.NE.(NVS+NVW/2)) GO TO 895
      V=((DEP2/NVW)-(DEP1/NVW))/(NVS*DT)
      DEP1=DEP2
      DEP2=0.D0
      NCOUNT=0
C
C  ESTABLISH MAXIMUM MELT-FRONT PENETRATION AND TIME
      VPROD=V*VAPRE
      IF(VPROD.GE.0.D0 .OR. ICOUNT.EQ.1) GO TO 895
      DEPMAX=DEPTH
      TMAX=TIME
      IFRMAX=IFRNT
```

```
      ICOUNT=1
  895 CONTINUE
C ------------------------------------------------------------------
C   TAKE NEXT TIME STEP
      TIME=TIME + DT
      TOUTG=TOUTG+DT
      TOUTD=TOUTD+DT
C ------------------------------------------------------------------
C   INCREASE TIME STEP TO MAXIMUM ALLOWED BY STABILITY CRITERION
      CPNMAX=1.00478D0+E(NMAX)*(-8.62645D-5
     &                          -2.51611D-7*E(NMAX))
      IF(T(NMAX).GT.1000) CPNMAX=1.D0
      DT=RATDX2*CPNMAX/K(NMAX)
C ------------------------------------------------------------------
C
C   TIME TO OUPUT TEMPERATURE AND ENERGY PROFILES ?
      IF(TOUTD .LT. DTOUTD) GO TO 3500
      TOUTD=0.0D0
C                          SUM ENERGY STORED IN FIRST NMAX+12 CELLS
      SUME=.5D0*E(NMAX)+.5D0*E(1)
      NXM1=NMAX-1
      DO 180 I=2,NXM1
        SUME=SUME+E(I)
  180 CONTINUE
      DO 190 I=1,12
        SUME=SUME+(E(NMAX+I)+E(NMAX+I-1))*
     &           (2**(I-3)+2**(I-2))
  190 CONTINUE
      SUME=(SUME-ET0)*DX*RH0
      SUMSX=SUMS1*DX*RH0
C                        SOME ENERGY ESCAPES OUT FIXED TEMP BACK BC
      PRINT 200 , TIME,N,V,DEPMAX,TMAX,DEPTH
      PRINT 211 , SUMSX,SUME
      PRINT 205
      PRINT 210 , (T(M2),M2=1,N)
      PRINT 215
      PRINT 210 , (E(M3),M3=1,N)
C
  200 FORMAT(' ',//'  TIME =',D13.5,' SEC   N=',I4,' V =',
     &       F8.1,/' DEPMAX=',D13.5,' TMAX=',D13.5,
     &       ' DEPTH=',D13.5)
  211 FORMAT(' ', 'LASER ENERGY IN =',D13.5,
     &          '    ENERGY IN NMAX+12 CELLS =',D13.5)
  210 FORMAT(' ',(12X,10(D10.4,1X)))
  225 FORMAT(' ',(12X,10(A1,11X)))
  205 FORMAT(' ',' TEMPERATURE')
  215 FORMAT(' ',' ENTHALPY')
  220 FORMAT(' ',' STATE A=AMORPHOUS C=CRYSTAL P=LARGE POLY',
     &       ' F=FINE POLY M=MUSHY L=LIQUID S=SUPERCOOLED')
C ------------------------------------------------------------------
C   TIME TO OUTPUT STATES ?
 3500 IF(TOUTG .LT. DTOUTG) GO TO 27
      TOUTG=0.D0
```

```
C  PREPARE OUTPUT STATE ARRAY
      DO 1200 I=1,N
      IPHASE=ISTATE(I)
      GO TO (13,23,33,43,53,53,53,83,93),IPHASE
   13 NSTATE(I)='C'
      GO TO 1200
   23 NSTATE(I)='P'
      GO TO 1200
   33 NSTATE(I)='F'
      GO TO 1200
   43 NSTATE(I)='A'
      GO TO 1200
   53 NSTATE(I)='M'
      GO TO 1200
   83 NSTATE(I)='L'
      GO TO 1200
   93 NSTATE(I)='S'
 1200 CONTINUE
C
C  OUTPUT LINE PRINTER GRAPH OF STATE VS TIME
      NG=MIN(N,100)
      WRITE(2,235) TIME,(NSTATE(M1),M1=1,NG)
  235 FORMAT(' ',D13.5,3X,100(A1))
C ---------------------------------------------------------------------
C
C  CHECK IF TIME TO STOP
      IF(TIME .LT. PULDUR) GO TO 27
      DO 1300 I=1,N
      IF(ISTATE(I).GT.4) GO TO 27
 1300 CONTINUE
C =====================================================================
C
C  WRITE OUT RESTART VECTORS
  112 WRITE(1,2100) TIME,N,DX,DT
      WRITE(1,2200) (T(M2),E(M2),ISTATE(M2),M2=1,N)
 2100 FORMAT(' ',D20.14,I5,D13.5,D13.5)
 2200 FORMAT(' ',(D20.14,5X,D20.14,5X,I2))
      CLOSE (1)
      CLOSE (2)
      CLOSE (6)
      STOP
      END
```

```
********************  SAMPLE INPUT FILE  ************************************
20,33,1.D-8,500,100,1.D-9,10.D-9                  N,NMAX,DX,IVS,IVW,DTOUTG,DTOUTD
33.5D-9,.3D0,1.D6,.58D0,.69D0,3                   TH,EL,ALPHA,RS,RL,ISHAPE
20.0D0,19.D-6,0                                   TINIT,XA,ISTART
4.D-9,8.D-9,2.33D0,1260.D0,1318.8D0,1310.D0       TP,TD,RH0,TA,HA,TN
1799.1D0,1410.D0,1.0D0,1500.D0                    HC,TC,CL,VMAX
```

ORNL-6242

INTERNAL DISTRIBUTION

1. L. S. Abbott
2. V. Alexiades
3. B. R. Appleton
4. M. J. Aziz
5. J. B. Bates
6. L. A. Boatner
7. J. F. Cooke
8. H. L. Davis
9. M. V. Denson
10. J. B. Drake
11-15. G. A. Geist
16. L. J. Gray
17. P. H. Green
18. G. R. Gruzalski
19-21. R. F. Harbison
Mathematical Sciences Library
22. M. T. Heath
23. N. Herbots
24. D. C. Human
25. G. E. Jellison, Jr.
26. L. H. Jenkins
27. T. Kaplan
28. W. E. Lever
29. D. H. Lowndes
30. G. D. Mahan
31. F. C. Maienschein
32. D. N. Mashburn
33. T. K. Miller
34. T. J. Mitchell
35. F. A. Modine
36. M. E. Mostoller
37. O. S. Oen
38. S. J. Pennycook
39. M. Rasolt
40. J. B. Roberto
41. M. T. Robinson
42. B. C. Sales
43. B. Sernelius
44. A. D. Solomon
45. S. Thompson
46. J. Z. Tischler
47. J. C. Wang
48. R. C. Ward
49. C. W. White
50. M. K. Wilkinson
51. S. P. Withrow
52-57. R. F. Wood
58. F. W. Young, Jr.
59. P. W. Dickson, Jr.(Consultant)
60. G. H. Golub (Consultant)
61. D. Steiner (Consultant)
62. Central Research Library
63. K-25 Plant Library
64. ORNL Patent Office
65. Y-12 Technical Library
Document Reference Section
66. Laboratory Records — RC
67-68. Laboratory Records Department

EXTERNAL DISTRIBUTION

69. Dr. Martin von Allmen, Institute of Applied Physics, University of Bern, Sidlerstrasse 5, CH-3012 Bern, Switzerland

70. Dr. Donald M. Austin, Division of Engineering, Mathematical and Geo-Sciences, Office of Basic Energy Sciences, Germantown Building, J-311, Department of Energy, Washington, D.C. 20545

71. Professor Shlomo Breuer, Department of Mathematics, Reusselaer Polytechnical Institute, Troy, N.Y.

72. Professor J. R. Cannon, Mathematics Department, Washington State University, Pullman, Washington 99164

73. Dr. T. C. Chawla, Building 208, Argonne National Laboratory, 9700 South Cass Avenue, Argonne, IL 60439

74. Dr. James S. Coleman, Division of Engineering, Mathematical and Geo-Sciences, Office of Basic Energy Sciences, Department of Energy, ER-17, MC G-256, Germantown, Washington, D.C. 20545

75. Dr. Sam Coriell, U.S. National Bureau of Standards, Mathematical Analysis Section, IBM, Washington, D.C. 20234

76. Professor John Crank, School of Mathematical Studies, Brunel University, Kingstone Lane, Uxbridge, UB8 3PH, Middlesex, ENGLAND

77. Professor Anna Crowley, Department of Mathematics, Royal Military College, Swindon, Wilts SN6-8LA, Swindon 782551, GREAT BRITAIN

78. Professor Avner Friedman, Department of Mathematics, Northwestern University, Evanston, IL 60201

79. Dr. Jameo Greenberg, Applied Mathematical Sciences, Scientific Computing Staff, Office of Energy Research, Washington, D.C. 20545

80. Dr. Philomena G. Grodzka, Huntsville Research & Engineering Center, Lockheed Missiles & Space Company, Inc., 4800 Bradford Drive, Huntsville, AL 35805

81. Professor Eugene Isaacson, New York University, Courant Institute of Mathematical Sciences, 251 Mercer Street, New York, NY 10012

82. Dr. K. A. Jackson, AT&T Bell Laboratories, Murray Hill, New Jersey 07974

83. Dr. Ralph James, Sandia National Laboratory, Division 8341, P.O. Box 969, 7011 E. Avenue, Livermore, CA 94550

84. Dr. William King, ASW, Martin Marietta Corporation, 132 N. Chesapeake Avenue, Baltimore, MD 21225

85. Professor W. Kurz, Department of Materials Engineering, Swiss Federal Institute of Technology, Lausanne, Switzerland CH-1007

86. Professor U. Landman, School of Physics, Georgia Institute of Technology, Atlanta GA 30322

87. Professor J. S. Langer, Institute for Theoretical Physics, University of California, Santa Barbara CA 93106

88. Dr. Alex Lehoczky, ES72, Space Science Laboratory, NASA, Marshall Space Flight Center, Huntsville, AL 35812

89. Professor John R. Ockendon, Oxford University Computing Center, 19 Parks Road, OX13 P1, Oxford, ENGLAND

90. Dr. P. S. Peercy, Division 5112, Sandia Laboratories, Albuquerque, New Mexico 87185

91. Professor M. Primiccerio, Inst. Matematico U.Dini, Via Morgagni 67/A, I-50134 Firenze, ITALY

92. Dr. M. Rappaz, Department of Materials Engineering, Swiss Federal Institute of Technology, Lausanne, Switzerland CH-1007

93. Dr. Milton E. Rose, Director, ICASE, Mail Stop 132C, NASA Langley Research Center, Hampton, VA 23665

94. Dr. Robert Siegel, Head, Analytical Fluid Mechanics Section, NASA Lewis Research Center, Cleveland, OH 44135

95. Dr. Frank Szofran, ES72, Space Science Laboratory, NASA, Marshall Space Flight Center, Huntsville, AL 35812

96. Professor M. O. Thompson, Department of Materials Science, Cornell University, Ithaca, New York 14853

97. Dr. R. Trivedi, Department of Materials Science and Engineering, Iowa State University, Ames, Iowa 50011

98. Professor D. Turnbull, Division of Applied Sciences, Harvard University, Cambridge, MA 02138

99. Professor D. R. Uhlmann, Center for Materials Science and Engineering, Massachusetts Institute of Technology, Cambridge, MA 02139

100. Professor Eitan Wacholder, Department of Nuclear Engineering, The Technion, Israel Institute of Technology, Haifa, ISRAEL

101. Dr. R. T. Young, Energy Conversion Devices, 1675 West Maple Road, Troy, MI 48084

102-128. Technical Information Center, Department of Energy, Oak Ridge, Tennessee, 37831.

129. Office of Assistant Manager for Energy Research and Development, Department of Energy, ORO, Oak Ridge, TN 37831